

1 **Centennial to millennial climate variability in the far northwestern Pacific (off**  
2 **Kamchatka) and its linkage to the East Asian monsoon and North Atlantic from the Last**  
3 **Glacial Maximum to the Early Holocene**

4 Sergey A. Gorbarenko [1], Xuefa Shi [2, 3], Galina Yu. Malakhova [4], Aleksandr A. Bosin [1],  
5 Jianjun Zou [2, 3], Yanguang Liu [2, 3], Min-Te Chen [5],

6 [1] V.I. Il'ichev Pacific Oceanological Institute, Russia

7 [2] Key Laboratory of Marine Sedimentology and Environmental Geology, First Institute of  
8 Oceanography, SOA, Qingdao, China

9 [3] Laboratory for Marine Geology, Qingdao National Laboratory for Marine Science and  
10 Technology, Qingdao, China

11 [4] North-East Interdisciplinary Science Research Institute FEB RAS, Russia

12 [5] National Taiwan Ocean University

13 **Abstract**

14 High resolution reconstructions based on productivity proxies and magnetic properties of core  
15 LV63-41-2 (off Kamchatka) reveal prevailing centennial productivity/climate variability in the  
16 northwestern (NW) Pacific from the Last Glacial Maximum (LGM) to the Early Holocene (EH). The  
17 age model of the core is established by AMS  $^{14}\text{C}$  dating and by projections of AMS  $^{14}\text{C}$  data of the  
18 nearby core SO-201-12KL through correlation of the productivity proxies and relative paleomagnetic  
19 intensity. The resulting sequence of centennial productivity increases/climate warming events in the  
20 NW Pacific occurred synchronously with the East Asian Summer Monsoon (EASM) sub-interstadials  
21 during the LGM (4 events), Heinrich Event 1 (HE1) (4 events), Bølling/Allerød (B/A) warming (4  
22 events), and over the EH (4 events). Remarkable similarity of the sequence of the NW Pacific  
23 increased productivity events with the EASM sub-interstadials over the LGM-HE1 implies that the  
24 Siberian High is a strong and common driver. The comparison with the  $\delta^{18}\text{O}$  record from Antarctica  
25 suggests that another mechanism associated with the temperature gradient in the Southern  
26 Hemisphere may also be responsible for the EASM / NW Pacific centennial events over the LGM-  
27 HE1. During the B/A warming and resumption of the AMOC, clear synchronicity between the NW  
28 Pacific, EASM and Greenland sub-interstadials was mainly controlled by changes in the atmospheric  
29 circulation. During the EH the linkages between solar forcing, ocean circulation, and climate changes,  
30 likely, control the synchronicity of abrupt climate changes in the NW Pacific and North Atlantic. The  
31 sequence of centennial events recorded in this study is a persistent regional feature during the LGM-

32 EH, which may serve as a template in high resolution paleoceanography and sediment stratigraphy in  
33 the NW Pacific.

## 34 **1. Introduction**

35 Model simulations and proxy-based records have both led to contradictory results on the  
36 millennial-scale environmental variability in the northwestern (NW) Pacific and its underlying  
37 mechanisms during the last deglaciation. These model and proxy studies suggested either in-phase  
38 relationships of deglacial variability between the North (N) Atlantic and NW Pacific (Caissie et al.,  
39 2010; Chikamoto et al., 2012; Kienast and McKay, 2001; Seki et al., 2002) or out-of-phase responses  
40 (Gebhardt et al., 2008; Sarnthein et al., 2006). The in phase relationship has been attributed to rapid  
41 atmospheric teleconnections in the Northern Hemisphere on a decadal time scale (Max et al., 2012).  
42 The winter Arctic Oscillation (AO), which resembles the North Atlantic Oscillation, directly  
43 influences the surface air temperature and sea level pressure over the region northwards of 35°N in  
44 East Asia (Sung et al., 2006). The Siberian High (SH), an essential component of northern East Asian  
45 atmosphere system, significantly influences the East Asian Winter Monsoon (EAWM) (Wu and  
46 Wang, 2002), which in turn affect the environment of NW Pacific. When winter AO is in its positive  
47 phase, both winter SH and EAWM are weaker than their normal state and air temperature of the  
48 surface- the middle troposphere is higher than normal (Wu and Wang, 2002), which ameliorate the  
49 NW Pacific environment. The out-of-phase response, however, was proposed to be driven by a  
50 seesaw mechanism, with oceanic readjustments between the weakening of the Atlantic meridional  
51 overturning circulation (AMOC) and the strengthening of the Pacific meridional overturning  
52 circulation (Okazaki et al., 2010).

53 Records of  $\delta^{18}\text{O}$  from the Greenland ice cores revealed the Dansgaard - Oeschger (DO)  
54 millennial scale oscillations (interstadials and stadials) during the last glaciation (Dansgaard et al.,  
55 1993; Johnsen et al., 1992) and similar millennial scale events have also been identified in a number  
56 of terrestrial and marine records in other regions. For example, a synthesis of the last glacial pollen  
57 records from the European continent provides evidence that the warmer intervals in Europe  
58 correspond to millennial-scale interstadials in Greenland (Fletcher et al., 2010). Sediment cores from  
59 the N Pacific and its marginal seas have also shown abrupt, millennial scale climate and environment  
60 ameliorations, similar to interstadials in Greenland ice cores during the last glaciation. Records of  
61  $\delta^{18}\text{O}$  of planktic foraminifera (Kennett et al., 2000) and alkenone-derived sea surface temperature  
62 (SST) (Seki et al., 2002) from the Northeastern (NE) Pacific also exhibited millennial climate  
63 oscillations very similar in magnitude with DO cycles over the last glaciation. INTIMATE  
64 stratigraphy studies introduced the subdivision of the GI-1 into sub-interstadials GI-1a to GI-1e.  
65 Furthermore, the GS-2.1 was subdivided into sub-stadials GS-2.1a (during Heinrich Event 1, HE1),

66 GS-2.1b (Last Glacial Maximum, LGM), and GS-2.1c (Björck et al., 1998; Rasmussen et al., 2014).  
67 The sequence of abrupt warming and environmental ameliorations similar to DO interstadials in  
68 Greenland were also interpreted by using alkenone-derived SST (Harada et al., 2008) and  
69 geochemical, diatom and pollen data (Gorbarenko et al., 2004) in sediment cores investigated from  
70 the Okhotsk Sea. The Bering Sea was also characterized by climate and environmental oscillations  
71 corresponded to DO cycles based on productivity proxies, sediment density, opal content and  
72 micropaleontological records (Gorbarenko et al., 2005; Kim et al., 2011; Riethdorf et al., 2013;  
73 Schlung et al., 2013).

74 By comparing the dust content in the North Greenland Ice Core Project (NGRIP) ice core with  
75 that of the dust record in a sediment core from the subarctic N Pacific, Serno et al. (2015)  
76 demonstrated synchronicity of millennial scale changes in atmospheric circulation between the N  
77 Pacific and the Greenland during the last 27 ka (Serno et al., 2015). Previous studies also found the  
78 occurrence of increased export of productivity during the period of millennial scale climate and  
79 environmental ameliorations, correlated with DO interstadials, in the Okhotsk and Bering Seas  
80 (Gorbarenko et al., 2005; Kim et al., 2011; Riethdorf et al., 2013; Seki et al., 2004).

81 Recent studies on high-resolution and well-dated sediment cores from the subarctic NW  
82 Pacific, the Okhotsk Sea, and the western Bering Sea show the variations in SST during the last  
83 deglaciation similar to the NE Pacific and to the N Atlantic and Greenland temperature variability  
84 (Caissie et al., 2010; Max et al., 2012; Seki et al., 2002). These studies suggest a close linkage to  
85 deglacial variations in AMOC associated with rapid atmospheric teleconnection, which were  
86 responsible for a quasi-synchronous SST pattern between the N Atlantic and N Pacific during the last  
87 deglaciation. Furthermore, a recent study by Praetorius and Mix (2014), based on multi-decadal-  
88 resolution foraminiferal  $\delta^{18}\text{O}$  records from the Gulf of Alaska, revealed a synchronicity of rapid  
89 climate shifts between the N Atlantic/Greenland (NGRIP record) and the NE Pacific between 15.5  
90 and 11 ka. During the Holocene and HE1, inverse relationships between the N Atlantic and the N  
91 Pacific are suggested by Praetorius and Mix (2014), while the short-term variability is either not  
92 sufficiently resolved or decoupled. A lack of high resolution records in the NW Pacific prohibits a  
93 precise assessment of any possible climatic teleconnection between the N Pacific and N Atlantic.

94 Besides centennial-millennial oscillations reported during the last glacial periods, centennial  
95 precipitation anomalies from LGM to the Holocene have also been reported in cave stalagmite  $\delta^{18}\text{O}$   
96 records of the East Asian monsoon (Dykoski et al., 2005; Wang et al., 2001, 2005, 2008; Yuan et al.,  
97 2004). Furthermore, the timing and pattern of variability during the Early Holocene (EH) regional  
98 climate changes are still under debate. In particular, though the EH climate has started from a strong  
99 warming in most cases, a Hani peat  $\delta^{18}\text{O}$  record from NE China instead suggest a centennial cooling

100 event which is primarily superimposed on a long-term warming trend during the Holocene (Hong et  
101 al., 2009).

102 Here we present high resolution results of productivity proxies, sediment magnetic properties,  
103 and lithological composition of a sediment core LV 63-41-2 (hereinafter, 41-2) (off Kamchatka) from  
104 the NW Pacific. Our records reveal a sequence of centennial productivity/climate variability from 20  
105 ka to 8 ka. An age model of core 41-2 was constructed using accelerator mass spectrometry (AMS)  
106  $^{14}\text{C}$  dating and by correlating the productivity events and relative paleomagnetic intensity (RPI)  
107 variability with those of the well-dated nearby core SO-201-12KL (hereinafter, 12KL) (Max et al.,  
108 2012, 2014). Using robust age controls, we establish a tight linkage between the centennial events  
109 with higher productivity in the NW Pacific and the sub-interstadial strengthened East Asian summer  
110 monsoon (EASM) expressed in cave stalagmite  $\delta^{18}\text{O}$  records. These results enable further  
111 investigation of any mechanisms in controlling the in phase relationships of the centennial variability  
112 in the NW Pacific / EASM and those underlying the Greenland / N Atlantic and Antarctic climate  
113 changes during the LGM through EH.

## 114 **2 Materials and methods**

115 Sediment core 41-2 (52°34' N, 160°01' E; water depth: 1924 m) was recovered from the NW  
116 Pacific off Kamchatka Peninsula during the Russian-Chinese Joint Expedition on R/V “Akademik  
117 M.A. Lavrentyev” in 2013. The length of the core is 467 cm. In order to establish the age model of  
118 core 41-2, we also analyzed paramagnetic magnetization and chlorin content in core 12KL (53°59' N,  
119 162°23' E), which has been dated well by Max et al. (2012, 2014).

### 120 **2.1 Coarse fraction**

121 Terrigenous materials are mainly transported by sea ice in the studied region and therefore the  
122 CF and magnetic susceptibility (MS) of sediments (Gorbarenko et al., 2003, 2012; Lisitzin, 2002;  
123 Sakamoto et al., 2005), can be used as a proxy for ice rafted debris (IRD). Semi-quantitative estimates  
124 of terrigenous and volcanic particles (tephra) in the CF allow the determination of core intervals with  
125 insignificant amounts of tephra, and therefore intervals with implications for CF and MS as an IRD  
126 index. Semi-quantitative estimates of major components in the sediment CF, including terrigenous  
127 and volcanic particles, benthic and planktic foraminifera shells, diatom frustules, and radiolarian  
128 skeletons on a twelve-point scale, were made by using a microscope for roughly estimating the  
129 proportions of different components in the sediment (Rothwell, 1989).

130 The weight percentage of coarse fraction (CF; 63-2000  $\mu\text{m}$ ) was obtained at 1 cm interval after  
131 wet sieving the sediment and calculated as a ratio of CF weight to the total weight of dry bulk  
132 sediment.

## 133 2.2 Chlorin

134 Chlorin content is assumed to reflect changes in primary surface ocean productivity, because  
135 continental-derived chlorophyll contributes insignificantly to its composition in deep marine  
136 sediment (Harris et al., 1996). The chlorin content in core 41-2 was measured by a Shimadzu UV-  
137 1650PC spectrophotometer at 1 cm resolution, and at 2 cm resolution in core 12KL, respectively,  
138 using same analytical reagents and pretreatment procedures proposed by Harris et al. (1996).

## 139 2.3 Total organic carbon (TOC), calcium carbonate (CaCO<sub>3</sub>), and color b\*

140 Contents of TOC, CaCO<sub>3</sub>, and biogenic opal in deep sea sediments are usually used as key  
141 parameters to assess paleoproductivity (Berger et al., 1989; Narita et al., 2002; Prah1 et al., 1989; Seki  
142 et al., 2004). The color b\* values correlate well with the changes in biogenic opal content in sediment  
143 cores (Nürnberg and Tiedemann, 2004) and are widely used as a paleoproductivity proxy in the NW  
144 Pacific and its marginal seas (Gorbarenko et al., 2012; Max et al., 2012; Riethdorf et al., 2013).

145 Total carbon and inorganic carbon contents in core 41-2 were measured at every 2 cm throughout  
146 the core by Coulometry using an AN-7529 analyzer in the same way, which has been reported by  
147 Gorbarenko et al. (1998). TOC content was determined by calculating the difference between total  
148 carbon and inorganic carbon content. Color b\* index (psychometric yellow–blue chromaticness) was  
149 measured with 1 cm resolution using a Minolta CM-2002 color reflectance spectrophotometer  
150 (Harada, 2006).

## 151 2.4 Radiocarbon dating (AMS <sup>14</sup>C)

152 AMS <sup>14</sup>C-ages were measured in monospecific samples of the planktic foraminifera  
153 *Neogloboquadrina pachyderma* sinistral (*N. pachyderma* sin.) from the 125–250 μm fraction, and  
154 benthic foraminifera *Epistominella pacifica*, and *Uvigerina parvocostata* from the 250–350 μm  
155 fraction of the core. The radiocarbon dating was performed by Dr. John Southon at the Keck Carbon  
156 Cycle AMS Facility (UCIAMS) in the Earth System Science Department of the University of  
157 California, USA.

158 The constant reservoir age (900 ± 250 yr) of the NW Pacific surface water (Max et al., 2012)  
159 was adopted in this study to convert the <sup>14</sup>C data into calendar ages by using Calib Rev 6.0 (Stuiver  
160 and Reimer, 1993) with Marine13 calibration curve (Reimer et al., 2013) to establish consistent AMS  
161 <sup>14</sup>C chronologies between cores 41-2 and 12KL. When using benthic foraminifera for AMS <sup>14</sup>C dating  
162 on the cores, an age difference of 1400 yrs is taken between coexisting benthic and planktic  
163 foraminifera ages (Max et al., 2014).

## 164 2.5 Magnetic properties

165 Variations in the Earth's magnetic field, recorded by RPI, presents an independent chronological  
166 instrument of marine and continental sediments (Channell et al., 2009), and is widely used for  
167 sediment correlation and chronology determination (Kiefer et al., 2001; Riethdorf et al., 2013). The  
168 sediment paramagnetic magnetization (PM) was formed in marine sediments in the open NW Pacific  
169 by silicate, paramagnetic iron sulphide (FeS), and fine clay minerals, the main part of which was  
170 transported from land as an eolian dust through atmospheric circulation by westerly jets (Serno et al.,  
171 2015). Therefore, the sediment PM may serve as a proxy for the land aridity and atmosphere  
172 circulation pattern changes. The volume MS of sediments was mainly formed by ferromagnetic  
173 minerals delivered together with terrigenous materials from adjacent land by sea ice, which is the  
174 main transport agent of clastic materials into the NW Pacific and its marginal seas (Gorbarenko et al.,  
175 2003; Lisitzin, 2002; Sakamoto et al., 2005).

176 The sediment magnetic properties were measured at 2.2 cm resolution in cores 41-2 and 12KL.  
177 MS of these samples was measured by an AGICO MFK1-FA device. The characteristic of remanent  
178 magnetization (ChRM) of the samples was measured in the same way by studying the stability of  
179 natural remanent magnetization (NRM) in an alternative magnetic fields of up to 80-100 mT on the  
180 basis of analysis of Zijderveld vector plots, using an AGICO LDA-3A device and rock-generator  
181 AGICO JR-5a (Zijderveld, 1964). The module and direction of NRM were measured on a JR-5A  
182 rock-generator after the stepwise demagnetization of reference samples by alternating magnetic fields  
183 with vanishing amplitude (Malakhov et al., 2009). Ahysteretic remanent magnetization (ARM) was  
184 generated using an AGICO AMU-1A device and measured using the JR-5A rock-generator. The RPI  
185 of the studied core was determined by the normalization of the ChRM after demagnetization at 20  
186 mT by ARM (ChRM/ARM) (Tauxe, 1993). The sediment PM was measured for each sample from  
187 curves of magnetic hysteresis by a J Meter coercitive spectrometer at Kazan State University, Kazan,  
188 Russia (Enkin et al., 2007; Jasonov et al., 1998).

## 189 **2.6 In-situ X-ray fluorescence core scanning**

190 Previous studies have shown that the non-destructive, high resolution X-ray fluorescence (XRF)  
191 measurements of biogenic barium, bromine and silica (Ba-bio, Br-bio, and Si-bio, respectively) by a  
192 core scanner or synchrotron radiation are consistent with analytically measured contents of Ba-bio,  
193 TOC, and biogenic opal, respectively, and therefore may be used as paleoproductivity proxies  
194 (Goldberg et al., 2005; Nürnberg and Tiedemann, 2004; Riethdorf et al., 2016). Ba-bio is formed  
195 during the decay of organic matter in the water column and the uptake of Ba in settling particles  
196 (Dymond et al., 1992), and has been previously used as a proxy of productivity (Goldberg and  
197 Arrhenius, 1958; McManus et al., 1998). Si-bio, related with biogenic opal in deep sea sediments, is  
198 usually used as a key parameter to assess paleoproductivity (Berger et al., 1989; Narita et al., 2002;

199 Seki et al., 2004). Br-bio content measured using a core scanner is strongly correlated with TOC  
200 variability (Riethdorf et al., 2013) and therefore may also be used as a paleoproductivity proxy.

201 The elemental composition of core 41-2 was measured as peak area in counts per second at 0.5  
202 cm resolution using the Itrax XRF core scanner at the First Institute of Oceanography, State Oceanic  
203 Administration, China. The Itrax XRF core scanner was set at 20 s count times, 30 kV X-ray voltage,  
204 and an X-ray current of 20 mA. Though absolute elemental concentrations are not directly available  
205 from the micro-XRF measurements, the count values can be used as estimates of the relative  
206 concentrations. The count values may be influenced by changes in the physical properties of the  
207 sediment, such as the water content and surface roughness of the core (Röhl and Abrams, 2000).  
208 However, the grain size of the 41-2 core is rather fine and the surface has been processed to be as flat  
209 as possible to minimize any effects from changing physical properties or roughness during the  
210 scanning.

211 In this study, attention was paid to the XRF scanning results for estimating the productivity  
212 proxies such as Ba-bio, Br-bio and Si-bio contents in our sediment core. The content of Ba-bio was  
213 estimated by the subtraction of its terrigenous component from the total Ba concentration in sediment  
214 (Ba-tot). The terrigenous component was, in turn, calculated from empirical regional  $(Ba/Al)_{ter}$  ratios  
215 in the sediment core with the lowest Ba-tot contents multiplied on relative Al content:

216  $Ba-bio = Ba-tot - (Ba/Al)_{ter} * Al$  (Goldberg et al., 2005).

217 The contents of Br-bio and Si-bio were calculated in the same way.

### 218 **3. Results**

#### 219 **3.1 Productivity events**

220 Down-core variability of all productivity proxies (color  $b^*$  and contents of TOC, chlorin,  
221  $CaCO_3$ , Ba-bio, Si-bio, and Br-bio) in core 41-2 is presented in Fig. 2. Taking the available AMS  $^{14}C$   
222 data into account (Table 1), the middle part of the core (the interval ~315-230 cm) with increased  
223 contents/values of all productivity proxies could be chronologically assigned to the Bølling/Allerød  
224 (B/A) warming right after the late last glaciation (467-315 cm). A decreased trend of productivity  
225 records at the interval of ~230-190 cm is likely associated with the YD cooling and the subsequent  
226 high productivity trend in the upper 190 cm is presumably related to the Holocene warming (Fig. 2).  
227 We interpret that the climate became warmer in the NW Pacific during the B/A period, terminating  
228 the last glaciation, then it reversed to the cooling during the Younger Dryas (YD) followed by the  
229 significant warming throughout the Holocene. This climate sequence has been well-documented by  
230 the  $\delta^{18}O$  records of the Greenland ice cores and climate records from the N Atlantic (Bond et al.,

231 2001; Dansgaard et al., 1993; Johnsen et al., 1992; Stuiver et al., 1995), by classical sequence of  
232 European pollen zone (Nilsson, 1983) and by well-dated pollen biome records of the southern Siberia  
233 (Bezrukova et al., 2010; Tarasov et al., 2009). The above mentioned patterns of climate variability  
234 during the LGM–EH in moderate-high latitudes of the Northern Hemisphere is consistent with the N  
235 Pacific and its marginal seas, evidenced by the alkenone- derived SST (Barron et al., 2003; Max et  
236 al., 2012) and pollen records (Gorbarenko et al., 2003, 2004). The significant increase in productivity  
237 in the NW Pacific during the B/A was likely achieved by additional nutrient input into the euphotic  
238 layer due to accelerated sea level rise (Siddall et al., 2010) accompanied by the supply of organic  
239 matter from the submerged shelf and by prolonged blooming season due to the warming that is a  
240 common paleoceanography feature of the N Pacific and its marginal seas (Barron et al., 2003, 2009;  
241 Caissie et al., 2010; Galbraith et al., 2007; Gorbarenko, 1996; Gorbarenko et al., 2005; Gorbarenko  
242 and Goldberg, 2005; Keigwin, 1998; Keigwin et al., 1992; Max et al., 2012; Seki et al., 2004).

243 In core 41-2, the temporal resolutions of measured color  $b^*$ , chlorin, TOC,  $\text{CaCO}_3$  and magnetic  
244 parameters (PM, MS, and RPI), and Ba-bio, Br-bio, and Si-bio are nearly 30 years, 15 years, and 60  
245 years respectively. The resolution is high enough to allow us to detect the centennial scale  
246 productivity variability in the NW Pacific. However, not all productivity proxies change  
247 synchronously (Fig. 2).

248 Each productivity proxy has its own specific limitations and peculiarities in response to the  
249 environmental and primary productivity changes. For example, carbonaceous fossils (planktic  
250 foraminifera and coccolithophorids) rain from the euphotic layer, exported by primary production,  
251 and they provide the main carbonate input into the sediment. However, the  $\text{CaCO}_3$  content in the deep  
252 sea sediment is also governed by climatically forced variability in the deep water chemistry and  
253 carbonate ion concentration ( $\text{CO}_3^{2-}$ ), resulting in different carbonate preservation in the past (Yu et  
254 al., 2013). As for the Ba-bio proxy, Jaccard et al. (2010) suggest that in the highly productive areas,  
255 barite dissolution has been observed under suboxic conditions, precluding its application as a  
256 quantitative proxy to reconstruct past changes in export production. Although it has been suggested  
257 that biogenic opal and TOC contents are responsible for the accumulation of siliceous fossils, and  
258 siliceous plus carbonaceous fossils with other organic remains, respectively (Berger et al., 1989), they  
259 vary in different ways at various periods in sediments of the NW Pacific and its marginal seas. For  
260 example, biogenic opal content in the Okhotsk Sea significantly lags the TOC changes during the last  
261 deglaciation—Late Holocene interval (Gorbarenko et al., 1998; Seki et al., 2004). TOC content in the  
262 hemipelagic sediment includes the organic carbon formed by marine primary production, and the  
263 terrigenous organic material delivered from land. Although it was suggested that color  $b^*$  values  
264 correlate well with the changes in biogenic opal content in sediment cores (Nürnberg and Tiedemann,



265 2004), the measured color  $b^*$  in core 41-2 do not change synchronously with Si-bio content in the  
266 entire length of the core (Fig. 2). The presentation of a wide range of productivity records allows us  
267 to evaluate the discrepancy among proxies. In addition, the combination of proxies provides a more  
268 reliable way for evaluating the productivity changes.

269 For the statistical assessment of the centennial productivity variability, a stack of productivity  
270 proxies is calculated. It is an average of the normalized data of each proxy with equal weight (Fig.  
271 2). Data from the productivity stack were detrended by subtracting long-term periodicity that allow  
272 us to determine the sequence of centennial productivity events with higher productivity throughout  
273 the studied core and events with lower productivity during the EH based on the seven productivity  
274 proxies measured (Fig. 2). The calculated productivity stack has high negative correlation with PM  
275 of sediments ( $r = -0.63$ ). This indicates that centennial events with increased productivity occurred  
276 during weakening of dust delivery and deposition in the NW Pacific by atmospheric circulation  
277 associated with abrupt climate warming. Such causal linkages between centennial productivity  
278 increases and abrupt climate warming in the NW Pacific is also consistent with millennial scale  
279 productivity /climate oscillations during the DO interstadials found in the Okhotsk and Bering Seas  
280 (Gorbarenko et al., 2005; Kim et al., 2011; Riethdorf et al., 2013; Seki et al., 2004). As a result, the  
281 records of different productivity proxies and the detrended productivity stack show eight short-term  
282 events with higher productivity occurred during the LGM and HE1 and 4 events during the B/A  
283 warming. During the EH, productivity records show 4 events of lower and higher productivity,  
284 respectively (Fig. 2).

285 It is noted that a low productivity event at ~9.1 ka (Table 1) is well-correlated with the 9.3 ka  
286 cold event recorded in NGRIP (Rasmussen et al., 2014). Moreover, a low productivity event  
287 identified at depth of 105-110 cm also correspond to the 8.2 ka cold event, a well-known  
288 chronostratigraphic marker in the Early to Middle Holocene boundary (Walker et al., 2012).

### 289 **3.2. Age model**

290 The RPI, productivity stack and PM of core 41-2 were compared with the RPI, several  
291 productivity proxies, and PM records of nearby core 12KL (Fig. 3). The color  $b^*$  index and Ca (analog  
292 of  $\text{CaCO}_3$  content) of core 12KL were obtained from Max et al. (2012, 2014). The correlation of the  
293 centennial productivity events between cores was provided by comparison of productivity stack of  
294 core 41-2 with productivity proxies of core 12KL and by comparison of the RPI and PM curves. An  
295 age model of core 41-2 was constructed using all available AMS  $^{14}\text{C}$  data, with additional age control  
296 points identified by correlating the centennial productivity events, RPI and PM of the studied core  
297 with those of the well-dated adjacent core 12KL (Max et al., 2012, 2014) (Fig. 3). The age tuning

298 used in this study assumes a synchronous pattern of productivity, RPI and PM variability in the NW  
299 Pacific since the last glacial, especially for closely-located cores. Therefore, the centennial variability  
300 of productivity proxies with increased productivity events, RPI of Earth's magnetic field, and PM  
301 identified in cores 41-2 and 12KL have to be closely matched in both cores over the last glaciation—  
302 B/A warming to the EH (Fig. 3). It was noted that the available age model for core 12KL (the  
303 Tiedemann/Max age model) (Max et al., 2012, 2014) was based on the AMS  $^{14}\text{C}$  data and correlation  
304 of color  $b^*$  index with the NGRIP  $\delta^{18}\text{O}$  curve. For adopting this age model to Core 41-2, the AMS  
305  $^{14}\text{C}$  data of core 12KL were projected to Core 41-2 according to the correlation of related productivity  
306 events, RPI and PM (Fig. 3). The color  $b^*$  minimum in core 12KL at a depth of 706 cm, which  
307 correlates with a minimum in the NGRIP  $\delta^{18}\text{O}$  record at 16.16 ka, is also clearly correlated with the  
308 color  $b^*$  minimum in core 41-2 at a depth of 348 cm (Fig. 3). All correlated AMS  $^{14}\text{C}$  data points are  
309 also well-matched with the measured RPI curves of both cores (Fig. 3). Our four AMS  $^{14}\text{C}$  data are  
310 fairly close to the projected  $^{14}\text{C}$  data from core 12KL (Table 3) with age differences within  $\pm 0.1$  ka,  
311 confirming the validity of these key point projections. Here the use of  $^{14}\text{C}$  data of core 12KL is  
312 preferred, because this core has a higher sedimentation rate, and planktic foraminifera for these  
313 measurements were picked-up from intervals with higher Ca peaks, aiming to reduce the effect of  
314 bioturbation on the precision of age model.

315 A close temporal correlation of these NW Pacific increased productivity events with sub-  
316 interstadials in the EASM becomes apparent after projection of the radiocarbon data of both cores on  
317 absolute U-Th dated  $\delta^{18}\text{O}$  record of Chinese cave stalagmites (Wang et al., 2008) during 20–8 ka  
318 (Fig. 3). Such inferred synchronicity of abrupt NW Pacific productivity events and EASM sub-  
319 interstadials was used for further tuning of age model. This was achieved by fine-tuning of the  
320 increased productivity events with related sub-interstadials of  $\delta^{18}\text{O}$  Chinese stalagmites at a depth  
321 beyond the projected AMS  $^{14}\text{C}$  data (Fig. 3; Table 3).

322 The sequence of centennial events of increased productivity seems to have occurred in phase  
323 with decreasing of PM in both cores (Fig. 3), indicating a weakening of eolian dust transportation by  
324 atmospheric circulation in the study area due likely to climate warming, analogous with millennial  
325 scale forcing of dust transportation into the NW Pacific (Serno et al., 2015). Within the constructed  
326 age model of core 41-2, different productivity proxies and magnetic records, combined with similar  
327 data from core 12KL (Max et al., 2012, 2014) reveal a sequence of noticeable centennial events of  
328 increased productivity in the NW Pacific which occurred in phase with Chinese sub-interstadials (CsI)  
329 associated with stronger EASM or weaker EAWM (Wang et al., 2008) and changes in atmospheric  
330 circulation during 21–8 ka (Figs. 3 and 4).

331 These linkages suggest that centennial scale increased productivity events in the NW Pacific  
332 were likely associated with shifts of a warmer regional climate and/or higher nutrient availability in  
333 surface water, synchronous with CsI of the EASM. According to Wang et al. (2001), the interstadials  
334 of EASM are broadly correlated with regional climate warming. High resolution records presented  
335 here show clearly that four centennial-scale events of increased productivity/environmental  
336 amelioration correlated with CsI during the LGM, four events during HE1, four events during the  
337 B/A warming, and four events during the EH (Fig. 4; Table 2).

## 338 **4. Discussion**

### 339 *4.1 Productivity patterns during the LGM-HE 1*

340 Besides the centennial productivity/environmental events, similar NW Pacific productivity  
341 patterns are found in cores 41-2 and 12KL during the LGM and HE1 with some differences in  
342 different productivity proxies. During the LGM, most proxies demonstrate a minimum primary  
343 productivity in the NW Pacific without definite trends (Fig. 4). Severe environmental conditions in  
344 central Asia inferred from pollen data (Bezrukova et al., 2010) (Fig. 5) seem to have promoted an  
345 increase in winter sea ice formation and sea ice cover in NW Pacific, consistent with high IRD  
346 accumulation inferred from CF and MS records (Fig. 4), that might have inhibited productivity in the  
347 study area. It is also consistent with the minimum productivity in the NW Pacific due to strong  
348 stratification, preventing the supply of nutrients required to support productivity in surface waters  
349 (Gebhardt et al., 2008).

350 From 17.8 to 15.3 ka, the TOC and chlorin contents associated with the production of calcareous  
351 phytoplankton (mostly coccolithophores) show a significant increase concurrently to the diminished  
352 AMOC (McManus et al., 2004). The diminished AMOC resulted in a major cooling of the Northern  
353 Hemisphere and, most likely, reduced water evaporation in the N Atlantic and therefore Atlantic-  
354 Pacific moisture transport (Okazaki et al., 2010). This condition facilitates an overall increase in  
355 surface water salinity, and decrease in surface stratification in the N Pacific, promoting an intensified  
356 ventilation of the intermediate water. The observed trends of productivity proxies are in concord with  
357 strong intensification of the intermediate-depth water ventilation in the N Pacific during HE1 (Max  
358 et al., 2014). However, fairly constant  $\text{CaCO}_3$  values in both cores (water depth 1924–2145 m) during  
359 the LGM-HE1 do not indicate that the water ventilation penetrated to deep water in the N Pacific over  
360 that time interval, because carbonate concentration in the sediment is strongly constrained by the  
361 ventilation of bathed water (Yu et al., 2013). The productivity proxies such as Si-bio and color  $b^*$ ,  
362 associated with siliceous phytoplankton production (mostly diatoms), were low and do not show  
363 significant trends during HE1 up to ~15.3 ka (Figs. 2 and 4). The enhanced coverage of sea ice, shown  
364 by CF and MS records (Fig. 4), until 15.3 ka in the studied area probably lead to the large spring–

365 early summer surface water stratification which impeded production of diatom. Both CF and MS  
366 records may represent IRD changes over the LGM-YD because the input of volcanic materials  
367 estimated in CF was insignificant during 21-12 ka compared to that of the Holocene (Fig. 4).

368 A sharp increase in the NW Pacific primary production, and a rise in the diatom production  
369 since ~15.3 ka indicated by most productivity proxies and Si-bio and color b\* records with a peak at  
370 sub-interstadial GI1-e of B/A warming (Fig. 4), was likely induced by a decreased effect of sea ice  
371 and its spring melting, favoring a weakening of surface stratification. The timing of the decrease in  
372 the sea ice cover since ~15.3 ka is consistent with the regional surface water warming (Max et al.,  
373 2012). Such a pattern in productivity changes in the N Pacific and the Bering Sea during the  
374 glacial/interglacial transitions has been reported in previous studies (Caissie et al., 2010; Galbraith et  
375 al., 2007; Gebhardt et al., 2008; Gorbarenko, 1996; Keigwin, 1998) and was likely a persistent feature  
376 of the N Pacific and its realm, forced by the resumption of the AMOC at the B/A warming.

377

#### 378 *4.2 Centennial variations in productivity during the LGM-HE1-B/A*

379 The identification of potential linkages between centennial climate changes in the Northern  
380 Hemisphere (NW Pacific, EASM, and N Atlantic/Greenland) and the climate changes recorded in the  
381 Antarctic ice cores is important for deepening our understanding of the mechanisms responsible for  
382 the timing and spatial propagation patterns that resulted from abrupt variability in global climate and  
383 environmental system. In order to test these linkages, the centennial productivity/climate events in  
384 the NW Pacific outlined by the productivity stack are compared with records from the Northern  
385 Hemisphere ( $\delta^{18}\text{O}$  and  $\text{Ca}^{2+}$  of NGRIP,  $\delta^{18}\text{O}$  of EASM, N Atlantic IRD, Siberian climate) and from  
386 the Southern Hemisphere (Fig.5). It has been suggested that the nearly synchronous ice core  $\delta^{18}\text{O}$  and  
387  $\text{Ca}^{2+}$  millennial-scale changes reflect the shifting of the Greenland atmospheric dust loading, which  
388 is closely linked with the atmospheric circulation and climate changes in the high latitudes of the  
389 Northern Hemisphere, where the EASM plays an important role (Ruth et al., 2007).

390 Similarity of glacial millennial-scale climate variability recorded in Chinese cave stalagmites  
391 and Greenland ice cores (Sun et al., 2012; Wang et al., 2001) implies a plausible influence of high-  
392 latitude climate of the Northern Hemisphere on the EASM by atmospheric circulation changes.  
393 Several main elements of atmospheric circulation, including the Intertropical Convergence Zone  
394 (ITCZ), northern westerly jet, AO and the SH, were previously considered as potential mechanisms  
395 linking abrupt climate changes in the N Atlantic and East Asia (Jin et al., 2007; Nagashima et al.,  
396 2011; Sung et al., 2006; Timmermann et al., 2007).

397 Apparent similarity of centennial climate and environment variability between the NW Pacific  
398 productivity events, EASM and Greenland records (Fig. 5) allow us to suggest that mechanisms  
399 responsible for their teleconnection were the same as on millennial scales. The remarkable similarity  
400 of the sequence of NW Pacific productivity events with the sub-interstadials of EASM records during  
401 the LGM-HE1 (Fig. 5) implies a strong common driver. Wu and Wang (2002) concluded that SH has  
402 provided direct and significant influence on the EAWM, particularly by sea level pressure and  
403 northerly wind along the East Asian Coast. Simultaneously, the SH strongly influences the sea ice  
404 formation in the NW Pacific and marginal seas by similar mechanisms like the wind intensity  
405 controlled by pressure gradient and winter air temperature at sea level (Kimura and Wakatsuchi,  
406 1999). Records of CF and MS, related with IRD accumulation, show that studied area off Kamchatka  
407 was influenced by sea ice during the LGM-HE1 (Fig. 4). We propose that the enhancement of SH,  
408 associated with abrupt climate cooling, led to an increase in terrigenous material delivery by sea ice  
409 from the coast and to a decrease in primary productivity by shrinking of productive season between  
410 events with increased productivity.

411 Correlation of the centennial changes in the NW Pacific productivity events / CsIs with  
412 Greenland sub interstadials during the LGM-HE1 was mainly observed but less clear, due to the  
413 discrepancy in constructed age models and/or to possible differences in atmospheric teleconnections  
414 (Fig. 5). There are some differences between coeval  $\delta^{18}\text{O}$  values in the Summit and NGRIP ice cores  
415 during the LGM-HE1, which were likely controlled by changes in the N American Ice Sheet volume  
416 and N Atlantic sea-ice coverage, resulting in the meridional discrepancy in the  $\delta^{18}\text{O}$  of Greenland ice  
417 (Seierstad et al., 2014).

418 EPICA community members (2006) showed that methane synchronization of the EDML and  
419 the  $\delta^{18}\text{O}$  of NGRIP reveal one-to-one alignment of each Antarctic warming with a corresponding  
420 stadial in the Greenland ice cores, implying a bipolar seesaw mechanism on millennial time scales.  
421 Since it was shown that Chinese and Greenland interstadials have occurred synchronously (Wang et  
422 al., 2001), therefore, Chinese interstadials (CIs) were also, likely, related to the Antarctic cold events.  
423 For example, warmer conditions in the Antarctic during 23.6–24.3 ka (coeval with Chinese sub-  
424 stadial CsS-GS3-1) were synchronous with abrupt climate cooling and an increase in dust content in  
425 the Greenland ice cores NGRIP, coeval with HE2 of the N Atlantic, and in phase with the weakening  
426 of the EASM (GS/CS-3.1) (Fig.5). The Antarctic cooling after 23.4 ka was accompanied by warming  
427 in Greenland, with two sharp interstadials GI-2.2 and GI-2.1 (Rasmussen et al., 2014) and EASM  
428 interstadial CI-2 (Wang et al., 2001) (Fig. 5).

429 It has also been suggested that an index of monsoon intensity was controlled not only by the  
430 Northern Hemisphere temperature (“pull” on the monsoon, which is more intense during boreal warm

431 periods), but also by the pole-to-equator temperature gradient in the Southern Hemisphere (“push”  
432 on the monsoon, which is more intense during the boreal cold periods) that leads to enhanced boreal  
433 summer monsoon intensity and its northward propagation (Rohling et al., 2009; Rossignol-Strick,  
434 1985; Xue et al., 2004). Since EASM transports heat and moisture from the West Pacific Warm Pool  
435 (WPWP) to higher latitudes (Wang et al., 2001), the temperature gradient in the Southern Hemisphere  
436 “pushes” the northward propagation of EASM via the latitudinal/longitudinal migrations or  
437 expansion/contraction of the WPWP (Rohling et al., 2009; Xue et al., 2004). This also explains the  
438 difference in responses to the EASM and Greenland interstadials and sub-interstadials, because the  
439 migration of the WPWP may have occurred more slowly than the atmospheric circulation changes  
440 (Rohling et al., 2009; Xue et al., 2004). The changes in the  $\delta^{18}\text{O}$  records of Chinese stalagmites were  
441 more gradual than in the  $\delta^{18}\text{O}$  records of Greenland ice cores, and were more similar to the changes  
442 of Antarctic air temperature (Fig. 5). So, it is possible that forcing from the low latitudes “push effect”  
443 on the EASM was an additional mechanism in centennial productivity changes in the NW Pacific due  
444 to surface water amelioration. Although the time resolution of the Antarctic  $\delta^{18}\text{O}$  curve was not as  
445 high as ones from the Greenland and the EASM, records demonstrated in Figure 5 do not exclude  
446 one-to-one alignment of each Antarctic centennial cooling with related EASM sub-interstadial / NW  
447 Pacific productivity events.

448 We suggest that, in addition to the eight centennial productivity/environmental events during  
449 the LGM-HE1 established in the studied cores from the NW Pacific, other three abrupt  
450 productivity/climate events likely took place in the NW Pacific, synchronous with CsIs outlined by  
451 the  $\delta^{18}\text{O}$  records of Chinese stalagmites and the Greenland during the interval of 25–20 ka (namely  
452 CsI-GS2.1-11, CsI-GS2.1-10, and CsI-GS2.1-9) (Fig. 5).

453 During the B/A warming and resumption of the AMOC, four sub-interstadials (CsI-GI1-a to  
454 CsI-GI1-e) were clearly and simultaneously observed in the Greenland ice cores  $\delta^{18}\text{O}$  (Björck et al.,  
455 1998) and dust records and EASM sub-interstadials synchronously with centennial productivity /  
456 environment events of the NW Pacific (Fig. 5). It is consistent with enhancement of the “pull effect”  
457 on the intensified EASM and therefore amelioration of the NW Pacific during boreal warm periods,  
458 which implies a dominant control of Northern Hemisphere climate processes on the atmospheric  
459 circulation in high latitudes (Rohling et al., 2009). Related significant coeval changes in the  
460 atmosphere circulation with periodicity *ca* 0.4 ka exert strong influence on the climate and  
461 environment in ocean and continent of the Northern Hemisphere during the B/A (Bezrukova et al.,  
462 2010).

### 463 ***4.3 Centennial variations in productivity during the EH***

464 During the EH the records presented here show an alternation of the four NW Pacific centennial  
465 events with lower and four ones with higher productivity, namely as CsS-EH-1 -CsS-EH-4 and CsI-  
466 EH-1 - CsI-EH-4, respectively (Figs. 4 and 5; Table 2). Two low productivity events (CsS-EH-1 and  
467 CsS-EH-2) are likely correlated with Greenland cold events at 8.2 ka and 9.3 ka, respectively  
468 (Rasmussen et al., 2014). Also, the NW Pacific low productivity events (CsS-EH-1, CsS-EH-2 and  
469 CsS-EH-3) occurred synchronously with the EASM decrease and climate cooling recorded in  $\delta^{18}\text{O}$   
470 of the Dongge cave stalagmite D4 (Dykoski et al., 2005) (Fig. 5). Therefore it may be suggested that  
471 during the EH the NW Pacific events with higher / lower productivity had occurred coeval with  
472 climate warming / cooling as well. The pollen-based reconstruction of the variability of the vegetation  
473 / climate from a well-dated core from south Siberia (Lake Baikal region) (Bezrukova et al., 2010)  
474 demonstrated nearly the same pattern of centennial variability during the EH (Fig. 5). Well-dated,  
475 high resolution lithological and geochemical results from the Yanchi playa (NE China) also clearly  
476 showed a sequence of three sharp cooling events at 8.2 ka, 9.9–10.1 ka, and 11.0–11.2 ka (Yu et al.,  
477 2006), quasi-synchronous with the NW Pacific productivity / climate events CsS-EH-1, CsS-EH-3  
478 and CsS-EH-4. Yu et al. (2006) explained this correlation through linkages between the tropical  
479 Pacific and N Atlantic.

480 An alternation of the NW Pacific events with lower / higher productivity during the EH  
481 demonstrates a perfect correlation with periodicities of solar activity and the production of the  
482 cosmogenic nuclides  $^{14}\text{C}$  and  $^{10}\text{Be}$  (Reimer et al., 2004) (Fig. 5). The production rates of these  
483 cosmogenic nuclides and residual atmospheric  $\Delta^{14}\text{C}$  record are negatively correlated with total solar  
484 irradiance due to the strength of magnetic fields embedded into the solar wind (Hu et al., 2003). Small  
485 variations in solar irradiance could be responsible for pronounced changes in northern high-latitude  
486 climate and environments (Bond et al., 2001; Hu et al., 2003). The NW Pacific events of higher  
487 productivity occurred during increased solar irradiance and climate warming, indicating that  
488 variability of the solar irradiance was a potential driver of the climate and environmental changes in  
489 the NW Pacific during the EH. The low productivity / cold climate CsS-EH-2 event in records of  
490 atmospheric  $\Delta^{14}\text{C}$  and the Greenland  $\delta^{18}\text{O}$  ice core was marked by sharp cooling at its onset and  
491 termination with some warming during the transition (Fig. 5). The CsS-EH-4 event shows a similar  
492 pattern in records of productivity stack and  $\delta^{18}\text{O}$  of the Greenland and Dongge cave D4, indicating  
493 fine structure of these cold events.

494 The influence of variations in solar output on hydrography of surface ocean in the subpolar N  
495 Atlantic during the Holocene was reported by Bond et al. (2001). The variability of subpolar N  
496 Atlantic ice drifting, recorded as the percentage of hematite-stained grains (Bond et al., 2001), though  
497 having lower time resolution and dating precision compared with production of the cosmogenic

498 nuclides, is consistent with other centennial climate changes in the Northern Hemisphere during the  
499 EH (Fig. 5).

500 The high resolution records of an alternation of the NW Pacific events with lower / higher  
501 productivity related with climate cooling / warming, demonstrating that centennial scale climate  
502 events during the EH were similar between the N Atlantic and NW Pacific, possibly because of the  
503 close linkages of sun-ocean-climate, consistent with earlier conclusions (Bond et al., 2001; Hong et  
504 al., 2009; Hu et al., 2003).

#### 505 ***4.4 Cross-correlation of the N Atlantic-NW Pacific climate variability***

506 Since whether N Atlantic-NW Pacific climate and hydrological in-phase or out-of-phase  
507 linkages are still under debate, empirical data obtained from sediment cores off Kamchatka offer the  
508 provision for clarifying this issue at high resolution. Here we provide comparison of the productivity  
509 stack of core 41-2, responsible for NW Pacific environmental variability, and  $\delta^{18}\text{O}$  records of the  
510 NGRIP ice core, responsible for the Greenland / N Atlantic climate changes (Rasmussen et al., 2014).  
511 Cross correlation of these records using moving windows at 2000 years shows more significant  
512 synchronization (from -0.6 to -0.9) from 15.8 ka up to 10.8 ka confirming strong atmospheric  
513 teleconnections between the NW Pacific and the N Atlantic during this period (Fig. 6). Cross  
514 correlation during early (19 ka - 15.8 ka) and later periods (10.8 ka - 9 ka) indicates weak NW Pacific  
515 - N Atlantic linkages, but do not support the out-of-phased hypothesis.

516

### 517 **5. Conclusions**

518 This study presents high resolution records of productivity proxies (TOC,  $\text{CaCO}_3$ , chlorin,  
519 color b\*, Ba-bio, Br-bio and Si-bio), sediment lithological, and magnetic properties from sediment  
520 cores, 41-2 and 12KL, taken from the NW Pacific. Results presented here reveal 16 centennial  
521 regional productivity events during the LGM-EH (20–8 ka) in the NW Pacific. Four NW Pacific  
522 abrupt increased productivity events are linked to CsIs during the LGM (20–17.8 ka), four during HE  
523 1 (17.8–14.7 ka) and four during the B/A. An alternative occurrence of four centennial events with  
524 lower and higher productivity was established during the EH.

525 On the basis of the age models of cores 41-2 and 12KL, we suggest that NW Pacific centennial  
526 events of increased productivity occur synchronously with sub-interstadials of the EASM. These NW  
527 Pacific events and EASM sub-interstadials are positively correlated with Greenland abrupt warming,  
528 indicating an atmospheric teleconnection between the NW Pacific and the N Atlantic during the  
529 LGM-HE 1-B/A.

530 Remarkable similarity of the sequence of productivity events recorded in the NW Pacific with  
531 the EASM sub-interstadials during the LGM-HE1 implies that SH is a strong driver. The comparison



532 between our stacked productivity with the  $\delta^{18}\text{O}$  of the EPICA, NGRIP and EASM suggest that another  
533 mechanism associated with the temperature gradient in the Southern Hemisphere (“push effect”) may  
534 relate to the EASM sub-interstadials and subsequent variability in productivity events in the NW  
535 Pacific on centennial time scales during the LGM-HE1.

536 During the B/A warming and resumption of the AMOC, synchronicity between the  
537 productivity events, EASM sub-interstadials, and the  $\delta^{18}\text{O}$  and dust records in the NGRIP is consistent  
538 with enhancement of the “pull effect” on the monsoon's intensity, which implies a dominant control  
539 of atmospheric processes on the productivity and climate of the NW Pacific.

540 During the EH, the high resolution records of an alternation of productivity events with lower  
541 / higher productivity related with climate cooling / warming, reveal that centennial climate events  
542 were similar between the subpolar regions of the N Atlantic and NW Pacific, and were controlled by  
543 mechanisms of sun-ocean-climate linkages.

544 In summary, the NW Pacific results presented here indicate a tight linkage and coherent  
545 pattern of centennial - millennial scale climate changes during the LGM-EH, which may serve as a  
546 template in high resolution paleoceanography and sediment stratigraphy of the moderate-high  
547 latitudes in the NW Pacific.

548

#### 549 **Acknowledgements**

550 We are grateful to Drs. Ralf Tiedemann and Dirk Nürnberg (AWI, GEOMAR, Germany) for a  
551 long and fruitful cooperation, and for providing samples and the dataset of core 12KL. We are  
552 indebted to Dr. John Southon (USA) for the AMS  $^{14}\text{C}$  dating. We thank Dr. Selvaraj Kandasamy  
553 (Xiamen University) to correct the paper. This research work was supported by the RFBR (Russian  
554 Fund of Basic Research), Russian project (13-05-00296a, 16-55-53048 and 16-05-00127), Russian  
555 Federation budget (No 01201363042), the International Cooperation Project of Global Change and  
556 Ocean-Atmosphere Interaction (GASIGEOGE-04), National Natural Science Foundation of China  
557 (Grant Nos.: 41476056, 41611130042 and U1606401) and by International Cooperative Projects in  
558 polar regions (201613), and the Russia-Taiwan Research Cooperation projects (14-HHC-002 and 17-  
559 MHT-003).

#### 560 **References**

561 Barron, J. A., Heusser, L., Herbert, T. and Lyle, M.: High-resolution climatic evolution of coastal  
562 northern California during the past 16,000 years, *Paleoceanography*, 18(1),  
563 doi:10.1029/2002PA000768, 2003.

564 Barron, J. A., Bukry, D., Dean, W. E., Addison, J. A. and Finney, B.: *Paleoceanography of the Gulf*

565 of Alaska during the past 15,000 years: Results from diatoms, silicoflagellates, and geochemistry,  
566 *Mar. Micropaleontol.*, 72(3–4), 176–195, doi:10.1016/j.marmicro.2009.04.006, 2009.

567 Berger, W. H., Smetacek, V. S. and Wefer, G.: Ocean Productivity and Paleoproductivity - An  
568 Overview, in *Productivity of the Ocean: Present and Past*, pp. 1–34., 1989.

569 Bezrukova, E. V., Tarasov, P. E., Solovieva, N., Krivonogov, S. K. and Riedel, F.: Last glacial–  
570 interglacial vegetation and environmental dynamics in southern Siberia: Chronology, forcing and  
571 feedbacks, *Palaeogeogr. Palaeoclimatol. Palaeoecol.*, 296(1–2), 185–198,  
572 doi:10.1016/j.palaeo.2010.07.020, 2010.

573 Björck, S., Walker, M. J. C., Cwynar, L. C., Johnsen, S., Knudsen, K.-L., Lowe, J. J. and  
574 Wohlfarth, B.: An event stratigraphy for the Last Termination in the North Atlantic region based on  
575 the Greenland ice-core record: a proposal by the INTIMATE group, *J. Quat. Sci.*, 13(4), 283–292,  
576 doi:10.1002/(SICI)1099-1417(199807/08)13:4<283::AID-JQS386>3.0.CO;2-A, 1998.

577 Bond, G. C., Kromer, B., Beer, J., Muscheler, R., Evans, M. N., Showers, W., Hoffmann, S., Lotti-  
578 Bond, R., Hajdas, I. and Bonani, G.: Persistent solar influence on North Atlantic climate during the  
579 Holocene, *Science*, 294(5549), 2130–6, doi:10.1126/science.1065680, 2001.

580 Caissie, B. E., Brigham-Grette, J., Lawrence, K. T., Herbert, T. D. and Cook, M. S.: Last Glacial  
581 Maximum to Holocene sea surface conditions at Umnak Plateau, Bering Sea, as inferred from  
582 diatom, alkenone, and stable isotope records, *Paleoceanography*, 25(1), PA1206,  
583 doi:10.1029/2008PA001671, 2010.

584 Channell, J. E. T., Xuan, C. and Hodell, D. A.: Stacking paleointensity and oxygen isotope data for  
585 the last 1.5 Myr (PISO-1500), *Earth Planet. Sci. Lett.*, 283(1–4), 14–23,  
586 doi:10.1016/j.epsl.2009.03.012, 2009.

587 Chikamoto, M. O., Menviel, L., Abe-Ouchi, A., Ohgaito, R., Timmermann, A., Okazaki, Y.,  
588 Harada, N., Oka, A. and Mouchet, A.: Variability in North Pacific intermediate and deep water  
589 ventilation during Heinrich events in two coupled climate models, *Deep Sea Res. Part II Top. Stud.*  
590 *Oceanogr.*, 61–64, 114–126, doi:10.1016/j.dsr2.2011.12.002, 2012.

591 Dansgaard, W., Johnsen, S. J., Clausen, H. B., Dahl-Jensen, D., Gundestrup, N. S., Hammer, C. U.,  
592 Hvidberg, C. S., Steffensen, J. P., Sveinbjörn, Jouzel, J. and Bond, G. C.: Evidence for general  
593 instability of past climate from a 250-kyr ice-core record, *Nature*, 364(6434), 218–220,  
594 doi:10.1038/364218a0, 1993.

595 Dykoski, C. A., Edwards, R. L., Cheng, H., Yuan, D., Cai, Y., Zhang, M., Lin, Y., Qing, J., An, Z.  
596 and Revenaugh, J.: A high-resolution, absolute-dated Holocene and deglacial Asian monsoon

597 record from Dongge Cave, China, *Earth Planet. Sci. Lett.*, 233(1–2), 71–86,  
598 doi:10.1016/j.epsl.2005.01.036, 2005.

599 Dymond, J., Suess, E. and Lyle, M.: Barium in Deep-Sea Sediment: A Geochemical Proxy for  
600 Paleoproductivity, *Paleoceanography*, 7(2), 163–181, doi:10.1029/92PA00181, 1992.

601 Enkin, R. J., Baker, J., Nourgaliev, D., Iassonov, P. and Hamilton, T. S.: Magnetic hysteresis  
602 parameters and Day plot analysis to characterize diagenetic alteration in gas hydrate-bearing  
603 sediments, *J. Geophys. Res.*, 112(B06S90), 1–13, doi:10.1029/2006JB004638, 2007.

604 EPICA Community Members: One-to-one coupling of glacial climate variability in Greenland and  
605 Antarctica, *Nature*, 444(7116), 195–198, doi:10.1038/nature05301, 2006.

606 Favorite, F., Dodimead, A. J. and Nasu, K.: Oceanography of the Subarctic Pacific region, 1960-  
607 1971., 1976.

608 Fletcher, W. J., Sanchez Goñi, M. F., Allen, J. R. M., Cheddadi, R., Combourieu-Nebout, N.,  
609 Huntley, B., Lawson, I., Londeix, L., Magri, D., Margari, V., Müller, U. C., Naughton, F.,  
610 Novenko, E., Roucoux, K. and Tzedakis, P. C.: Millennial-scale variability during the last glacial in  
611 vegetation records from Europe, *Quat. Sci. Rev.*, 29(21–22), 2839–2864,  
612 doi:10.1016/j.quascirev.2009.11.015, 2010.

613 Galbraith, E. D., Jaccard, S. L., Pedersen, T. F., Sigman, D. M., Haug, G. H., Cook, M., Southon, J.  
614 R. and Francois, R.: Carbon dioxide release from the North Pacific abyss during the last  
615 deglaciation., *Nature*, 449(7164), 890–893, doi:10.1038/nature06227, 2007.

616 Gebhardt, H., Sarnthein, M., Grootes, P. M., Kiefer, T., Kuehn, H., Schmieder, F. and Röhl, U.:  
617 Paleonutrient and productivity records from the subarctic North Pacific for Pleistocene glacial  
618 terminations I to V, *Paleoceanography*, 23(4), doi:10.1029/2007PA001513, 2008.

619 Goldberg, E. D. and Arrhenius, G. O. S.: Chemistry of Pacific pelagic sediments, *Geochim.*  
620 *Cosmochim. Acta*, 13(2–3), 153–212, doi:10.1016/0016-7037(58)90046-2, 1958.

621 Goldberg, E. L., Gorbarenko, S. A., Shaporenko, A. D., Bosin, A. A., Leskov, V. Y. and Chebykin,  
622 E. P.: Instability of last glacial climate from SRXFA data for bottom sediments in the Okhotsk Sea,  
623 *Nucl. Instruments Methods Phys. Res. Sect. A Accel. Spectrometers, Detect. Assoc. Equip.*, 543(1),  
624 284–287, doi:10.1016/j.nima.2005.01.242, 2005.

625 Gorbarenko, S. A.: Stable Isotope and Lithologic Evidence of Late-Glacial and Holocene  
626 Oceanography of the Northwestern Pacific and Its Marginal Seas, *Quat. Res.*, 46(3), 230–250,  
627 doi:10.1006/qres.1996.0063, 1996.

628 Gorbarenko, S. A. and Goldberg, E. L.: Assessment of Variations of Primary Production in the Sea  
629 of Okhotsk, Bering Sea, and Northwestern Pacific over the Last Glaciation Maximum and  
630 Holocene, *Dokl. Earth Sci.*, 405(9), 1380–1383, 2005.

631 Gorbarenko, S. A., Chekhovskaya, M. P. and Southon, J. R.: Detailed environmental changes of the  
632 Okhotsk Sea central part during last Glaciation Holocene, *Oceanologia*, 38(2), 305–308, 1998.

633 Gorbarenko, S. A., Leskov, V. Y., Artemova, A. V., Tiedemann, R., Biebow, N. and Nürnberg, D.:  
634 Ice Cover of the Sea of Okhotsk during the Last Glaciation and Holocene, *Dokl. Earth Sci.*, 389(2),  
635 208–211, 2003.

636 Gorbarenko, S. A., Southon, J. R. J. ., Keigwin, L. D., Cherepanova, M. . and Gvozdeva, I. . G.:  
637 Late Pleistocene–Holocene oceanographic variability in the Okhotsk Sea: geochemical, lithological  
638 and paleontological evidence, *Palaeogeogr. Palaeoclimatol. Palaeoecol.*, 209(1–4), 281–301,  
639 doi:10.1016/j.palaeo.2004.02.013, 2004.

640 Gorbarenko, S. A., Basov, I. A., Chekhovskaya, M. P., Southon, J. R., Khusid, T. A. A. and  
641 Artemova, A. V.: Orbital and millennium scale environmental changes in the southern Bering Sea  
642 during the last glacial-Holocene: Geochemical and paleontological evidence, *Deep Sea Res. Part II*  
643 *Top. Stud. Oceanogr.*, 52(16–18), 2174–2185, doi:10.1016/j.dsr2.2005.08.005, 2005.

644 Gorbarenko, S. A., Harada, N., Malakhov, M. I., Velivetskaya, T. A., Vasilenko, Y. P., Bosin, A.  
645 A., Derkachev, A. N., Goldberg, E. L. and Ignatiev, A. V.: Responses of the Okhotsk Sea  
646 environment and sedimentology to global climate changes at the orbital and millennial scale during  
647 the last 350 kyr, *Deep Sea Res. Part II Top. Stud. Oceanogr.*, 61–64, 73–84,  
648 doi:10.1016/j.dsr2.2011.05.016, 2012.

649 Harada, N.: MIRAI cruise report MR06-04 Leg 1 and 2, JAMSTEC, Yokosuka. [Available at  
650 [http://www.godac.jamstec.go.jp/cruisedata/mirai/e/MR06-04\\_leg1.html](http://www.godac.jamstec.go.jp/cruisedata/mirai/e/MR06-04_leg1.html)], 2006.

651 Harada, N., Sato, M. and Sakamoto, T.: Freshwater impacts recorded in tetraunsaturated alkenones  
652 and alkenone sea surface temperatures from the Okhotsk Sea across millennial-scale cycles,  
653 *Paleoceanography*, 23(3), doi:10.1029/2006PA001410, 2008.

654 Harris, P. G., Zhao, M., Rosell-Melé, A., Tiedemann, R., Sarnthein, M. and Maxwell, J. R.: Chlorin  
655 accumulation rate as a proxy for Quaternary marine primary productivity, *Nature*, 383(6595), 63–  
656 65, doi:10.1038/383063a0, 1996.

657 Hong, Y. T., Hong, B., Lin, Q. H., Shibata, Y., Zhu, Y. X., Leng, X. T. and Wang, Y.: Synchronous  
658 climate anomalies in the western North Pacific and North Atlantic regions during the last 14,000  
659 years, *Quat. Sci. Rev.*, 28(9–10), 840–849, doi:10.1016/j.quascirev.2008.11.011, 2009.

660 Hu, F. S., Kaufman, D., Yoneji, S., Nelson, D., Shemesh, A., Huang, Y., Tian, J., Bond, G. C.,  
661 Clegg, B. and Brown, T. A.: Cyclic variation and solar forcing of Holocene climate in the Alaskan  
662 subarctic., *Science*, 301(5641), 1890–1893, doi:10.1126/science.1088568, 2003.

663 Jaccard, S. L., Galbraith, E. D., Sigman, D. M. and Haug, G. H.: A pervasive link between  
664 Antarctic ice core and subarctic Pacific sediment records over the past 800 kyrs, *Quat. Sci. Rev.*,  
665 29(1–2), 206–212, doi:10.1016/j.quascirev.2009.10.007, 2010.

666 Jasonov, P. G., Nurgaliev, D. K., Burov, B. V. and Heller, F.: A modernized coercivity  
667 spectrometer, *Geol. Carpathica*, 49(3), 2254–225, 1998.

668 Jin, L., Chen, F., Ganopolski, A. and Claussen, M.: Response of East Asian climate to  
669 Dansgaard/Oeschger and Heinrich events in a coupled model of intermediate complexity, *J.*  
670 *Geophys. Res.*, 112(D6), D06117, doi:10.1029/2006JD007316, 2007.

671 Johnsen, S. J., Clausen, H. B., Dansgaard, W., Fuhrer, K., Gundestrup, N., Hammer, C. U., Iversen,  
672 P., Jouzel, J., Stauffer, B. and Steffensen, J. P.: Irregular glacial interstadials recorded in a new  
673 Greenland ice core, *Nature*, 359(6393), 311–313, doi:10.1038/359311a0, 1992.

674 Keigwin, L. D.: Glacial-age hydrography of the far northwest Pacific Ocean, *Paleoceanography*,  
675 13(4), 323–339, doi:10.1029/98PA00874, 1998.

676 Keigwin, L. D., Jones, G. A. and Froelich, P. N.: A 15,000 year paleoenvironmental record from  
677 Meiji Seamount, far northwestern Pacific, *Earth Planet. Sci. Lett.*, 111(2–4), 425–440,  
678 doi:10.1016/0012-821X(92)90194-Z, 1992.

679 Kennett, J. P., Roark, E. B., Cannariato, K. G., Ingram, B. L. and Tada, R.: Latest quaternary  
680 paleoclimatic and radiocarbon chronology, Hole 1017E, Southern California margin, *Proc. Ocean*  
681 *Drill. Progr.*, 167, 249–254, 2000.

682 Kiefer, T., Sarnthein, M., Erlenkeuser, H., Grootes, P. M. and Roberts, A. P.: North Pacific  
683 response to millennial-scale changes in ocean circulation over the last 60 kyr, *Paleoceanography*,  
684 16(2), 179–189, doi:10.1029/2000PA000545, 2001.

685 Kienast, S. S. and McKay, J. L.: Sea surface temperature in the subarctic Northeast Pacific reflect  
686 millennial-scale climate oscillations during the last 16 kyr, *Geophys. Res. Lett.*, 28(8), 1563–1566,  
687 2001.

688 Kim, S.-J., Khim, B.-K., Uchida, M., Itaki, T. and Tada, R.: Millennial-scale paleoceanographic  
689 events and implication for the intermediate-water ventilation in the northern slope area of the  
690 Bering Sea during the last 71 kyrs, *Glob. Planet. Change*, 79(1–2), 89–98,

691 doi:10.1016/j.gloplacha.2011.08.004, 2011.

692 Kimura, N. and Wakatsuchi, M.: Processes controlling the advance and retreat of sea ice in the Sea  
693 of Okhotsk, *J. Geophys. Res.*, 104(C5), 11137, doi:10.1029/1999JC900004, 1999.

694 Lisitzin, A. P.: *Sea-Ice and Iceberg Sedimentation in the Ocean*, Springer, Berlin, Heidelberg.,  
695 2002.

696 Malakhov, M. I., Gorbarenko, S. A., Malakhova, G. Y., Harada, N., Vasilenko, Y. P., Bosin, A. A.,  
697 Goldberg, E. L. and Derkachev, A. N.: Petromagnetic parameters of bottom sediments as indicators  
698 of the climatic and environmental changes in the central zone of the Sea of Okhotsk during the last  
699 350 kyr, *Russ. Geol. Geophys.*, 50(11), 973–982, doi:10.1016/j.rgg.2009.10.006, 2009.

700 Max, L., Riethdorf, J.-R., Tiedemann, R., Smirnova, M., Lembke-Jene, L., Fahl, K., Nürnberg, D.,  
701 Matul, A. G. and Mollenhauer, G.: Sea surface temperature variability and sea-ice extent in the  
702 subarctic northwest Pacific during the past 15,000 years, *Paleoceanography*, 27(3),  
703 doi:10.1029/2012PA002292, 2012.

704 Max, L., Lembke-Jene, L., Riethdorf, J.-R., Tiedemann, R., Nürnberg, D., Kühn, H. and  
705 Mackensen, A.: Pulses of enhanced North Pacific Intermediate Water ventilation from the Okhotsk  
706 Sea and Bering Sea during the last deglaciation, *Clim. Past*, 10(2), 591–605, doi:10.5194/cp-10-  
707 591-2014, 2014.

708 McManus, J., Berelson, W. M., Klinkhammer, G. P., Johnson, K. S., Coale, K. H., Anderson, R. F.,  
709 Kumar, N., Burdige, D. J., Hammond, D. E., Brumsack, H.-J., McCorkle, D. C. and Rushdi, A.:  
710 Geochemistry of barium in marine sediments: implications for its use as a paleoproxy, *Geochim.*  
711 *Cosmochim. Acta*, 62(21–22), 3453–3473, doi:10.1016/S0016-7037(98)00248-8, 1998.

712 McManus, J. F., Francois, R., Gherardi, J.-M., Keigwin, L. D. and Brown-Leger, S.: Collapse and  
713 rapid resumption of Atlantic meridional circulation linked to deglacial climate changes., *Nature*,  
714 428(6985), 834–837, doi:10.1038/nature02494, 2004.

715 Nagashima, K., Tada, R., Tani, A., Sun, Y., Isozaki, Y., Toyoda, S. and Hasegawa, H.: Millennial-  
716 scale oscillations of the westerly jet path during the last glacial period, *J. Asian Earth Sci.*, 40(6),  
717 1214–1220, doi:10.1016/j.jseaes.2010.08.010, 2011.

718 Narita, H., Sato, M., Tsunogai, S., Murayama, M., Ikehara, M., Nakatsuka, T., Wakatsuchi, M.,  
719 Harada, N. and Ujiie, Y.: Biogenic opal indicating less productive northwestern North Pacific  
720 during the glacial ages, *Geophys. Res. Lett.*, 29(15), 22-1-22–4, doi:10.1029/2001GL014320, 2002.

721 Nilsson, T.: *The Pleistocene; Geology and Life in the Quaternary Ice Age*, D. Reidel, Dordrecht.,

722 1983.

723 North Greenland Ice Core Project members: High-resolution record of Northern Hemisphere  
724 climate extending into the last interglacial period, *Nature*, 431(7005), 147–151,  
725 doi:10.1038/nature02805, 2004.

726 Nürnberg, D. and Tiedemann, R.: Environmental change in the Sea of Okhotsk during the last 1.1  
727 million years, *Paleoceanography*, 19(4), PA4011, doi:10.1029/2004PA001023, 2004.

728 Okazaki, Y., Timmermann, A., Menviel, L., Harada, N., Abe-Ouchi, A., Chikamoto, M. O.,  
729 Mouchet, A. and Asahi, H.: Deepwater formation in the North Pacific during the Last Glacial  
730 Termination., *Science*, 329(5988), 200–204, doi:10.1126/science.1190612, 2010.

731 Praetorius, S. K. and Mix, A. C.: Synchronization of North Pacific and Greenland climates preceded  
732 abrupt deglacial warming, *Science*, 345(6195), 444–448, doi:10.1126/science.1252000, 2014.

733 Prah, F. G., Muehlhausen, L. A. and Lyle, M.: An organic geochemical assessment of  
734 oceanographic conditions at Manop Site C over the past 26,000 years, *Paleoceanography*, 4(5),  
735 495–510, doi:10.1029/PA004i005p00495, 1989.

736 Rasmussen, S. O., Bigler, M., Blockley, S. P., Blunier, T., Buchardt, S. L., Clausen, H. B.,  
737 Cvijanovic, I., Dahl-Jensen, D., Johnsen, S. J., Fischer, H., Gkinis, V., Guillevic, M., Hoek, W. Z.,  
738 Lowe, J. J., Pedro, J. B., Popp, T., Seierstad, I. K., Steffensen, J. P., Svensson, A. M., Vallelonga,  
739 P., Vinther, B. M., Walker, M. J. C., Wheatley, J. J. and Winstrup, M.: A stratigraphic framework  
740 for abrupt climatic changes during the Last Glacial period based on three synchronized Greenland  
741 ice-core records: refining and extending the INTIMATE event stratigraphy, *Quat. Sci. Rev.*, 106,  
742 14–28, doi:10.1016/j.quascirev.2014.09.007, 2014.

743 Reimer, P. J., Baillie, M. G. L., Bard, E., Beck, J. W., Bertrand, C. J. H., Blackwell, P. G., Buck, C.  
744 E., Burr, G. S., Cutler, K. B., Damon, P. E., Edwards, R. L., Fairbanks, R. G., Friedrich, M. and  
745 Guilderson, T. P.: IntCal04 terrestrial radiocarbon age calibration, 0–26 cal kyr BP, *Radiocarbon*,  
746 46(3), 1029–1058, 2004.

747 Reimer, P. J., Bard, E., Bayliss, A., Beck, J. W., Blackwell, P. G., Bronk Ramsey, C., Buck, C. E.,  
748 Cheng, H., Edwards, R. L., Friedrich, M., Grootes, P. M., Guilderson, T. P., Haflidason, H., Hajdas,  
749 I., Hatte, C., Heaton, T. J., Hoffmann, D. L., Hogg, A. G., Hughen, K. A., Kaiser, K. F., Kromer,  
750 B., Manning, S. W., Niu, M., Reimer, R. W., Richards, D. A., Scott, E. M., Southon, J. R., Staff, R.  
751 A., Turney, C. S. M. and van der Plicht, J.: IntCal13 and Marine13 Radiocarbon Age Calibration  
752 Curves 0–50,000 Years cal BP, *Radiocarbon*, 55(4), 1869–1887, doi:10.2458/azu\_js\_rc.55.16947,  
753 2013.

754 Riethdorf, J.-R., Nürnberg, D., Max, L., Tiedemann, R., Gorbarenko, S. A. and Malakhov, M. I.:  
755 Millennial-scale variability of marine productivity and terrigenous matter supply in the western  
756 Bering Sea over the past 180 kyr, *Clim. Past*, 9(3), 1345–1373, doi:10.5194/cp-9-1345-2013, 2013.

757 Riethdorf, J.-R., Thibodeau, B., Ikehara, M., Nürnberg, D., Max, L., Tiedemann, R., Yokoyama, Y.,  
758 Riethdorf, J.-R., Thibodeau, B., Ikehara, M., Nürnberg, D., Max, L., Tiedemann, R. and Yokoyama,  
759 Y.: Surface nitrate utilization in the Bering sea since 180kA BP: Insight from sedimentary nitrogen  
760 isotopes, *Deep Sea Res. Part II Top. Stud. Oceanogr.*, 125–126, 163–176,  
761 doi:10.1016/j.dsr2.2015.03.007, 2016.

762 Röhl, U. and Abrams, L. J.: High-resolution, downhole, and nondestructive core measurements  
763 from Sites 999 and 1001 in the Caribbean Sea: application to the Late Paleocene Thermal  
764 Maximum, in *Proceedings of the Ocean Drilling Program, 165 Scientific Results*, vol. 165, pp. 191–  
765 203, Ocean Drilling Program., 2000.

766 Rohling, E. J., Liu, Q. S., Roberts, a. P., Stanford, J. D., Rasmussen, S. O., Langen, P. L. and  
767 Siddall, M.: Controls on the East Asian monsoon during the last glacial cycle, based on comparison  
768 between Hulu Cave and polar ice-core records, *Quat. Sci. Rev.*, 28, 3291–3302,  
769 doi:10.1016/j.quascirev.2009.09.007, 2009.

770 Rossignol-Strick, M.: Mediterranean Quaternary sapropels, an immediate response of the African  
771 monsoon to variation of insolation, *Palaeogeogr. Palaeoclimatol. Palaeoecol.*, 49(3–4), 237–263,  
772 doi:10.1016/0031-0182(85)90056-2, 1985.

773 Rothwell, R. G.: The Smear Slide Method, in *Minerals and Mineraloids in Marine Sediments*, pp.  
774 21–24, Springer Netherlands, Dordrecht., 1989.

775 Ruth, U., Bigler, M., Röthlisberger, R., Siggaard-Andersen, M.-L., Kipfstuhl, S., Goto-Azuma, K.,  
776 Hansson, M. E., Johnsen, S. J., Lu, H. and Steffensen, J. P.: Ice core evidence for a very tight link  
777 between North Atlantic and east Asian glacial climate, *Geophys. Res. Lett.*, 34(L03706), 1–5,  
778 doi:10.1029/2006GL027876, 2007.

779 Sakamoto, T., Ikehara, M., Aoki, K., Iijima, K., Kimura, N., Nakatsuka, T. and Wakatsuchi, M.:  
780 Ice-rafted debris (IRD)-based sea-ice expansion events during the past 100 kyrs in the Okhotsk Sea,  
781 *Deep Sea Res. Part II Top. Stud. Oceanogr.*, 52(16–18), 2275–2301,  
782 doi:10.1016/j.dsr2.2005.08.007, 2005.

783 Sarnthein, M., Kiefer, T., Grootes, P. M., Elderfield, H. and Erlenkeuser, H.: Warmings in the far  
784 northwestern Pacific promoted pre-Clovis immigration to America during Heinrich event 1,  
785 *Geology*, 34(3), 141–144, doi:10.1130/G22200.1, 2006.



786 Schlung, S. A., Christina Ravelo, A., Aiello, I. W., Andreasen, D. H., Cook, M. S., Drake, M.,  
787 Dyez, K. A., Guilderson, T. P., LaRiviere, J. P., Stroynowski, Z. and Takahashi, K.: Millennial-  
788 scale climate change and intermediate water circulation in the Bering Sea from 90 ka: A high-  
789 resolution record from IODP Site U1340, *Paleoceanography*, 28(1), 54–67,  
790 doi:10.1029/2012PA002365, 2013.

791 Seierstad, I. K., Abbott, P. M., Bigler, M., Blunier, T., Bourne, A. J., Brook, E. J., Buchardt, S. L.,  
792 Buizert, C., Clausen, H. B., Cook, E., Dahl-Jensen, D., Davies, S. M., Guillevic, M., Johnsen, S. J.,  
793 Pedersen, D. S., Popp, T. J., Rasmussen, S. O., Severinghaus, J. P., Svensson, A. and Vinther, B.  
794 M.: Consistently dated records from the Greenland GRIP, GISP2 and NGRIP ice cores for the past  
795 104 ka reveal regional millennial-scale  $\delta^{18}\text{O}$  gradients with possible Heinrich event imprint, *Quat.*  
796 *Sci. Rev.*, 106, 29–46, doi:10.1016/j.quascirev.2014.10.032, 2014.

797 Seki, O., Ishiwatari, R. and Matsumoto, K.: Millennial climate oscillations in NE Pacific surface  
798 waters over the last 82 kyr: New evidence from alkenones, *Geophys. Res. Lett.*, 29(23), 59-1-59–4,  
799 doi:10.1029/2002GL015200, 2002.

800 Seki, O., Ikehara, M., Kawamura, K., Nakatsuka, T., Ohnishi, K., Wakatsuchi, M., Narita, H. and  
801 Sakamoto, T.: Reconstruction of paleoproductivity in the Sea of Okhotsk over the last 30 kyr,  
802 *Paleoceanography*, 19(1), doi:10.1029/2002PA000808, 2004.

803 Serno, S., Winckler, G., Anderson, R. F., Maier, E., Ren, H., Gersonde, R. and Haug, G. H.:  
804 Comparing dust flux records from the Subarctic North Pacific and Greenland: Implications for  
805 atmospheric transport to Greenland and for the application of dust as a chronostratigraphic tool,  
806 *Paleoceanography*, 30(6), 583–600, doi:10.1002/2014PA002748, 2015.

807 Siddall, M., Kaplan, M. R., Schaefer, J. M., Putnam, A., Kelly, M. A. and Goehring, B.: Changing  
808 influence of Antarctic and Greenlandic temperature records on sea-level over the last glacial cycle,  
809 *Quat. Sci. Rev.*, 29(3–4), 410–423, doi:10.1016/j.quascirev.2009.11.007, 2010.

810 Stuiver, M. and Reimer, P. J.: Extended 14C Data Base and Revised Calib 3.0 14C Age Calibration  
811 Program, *Radiocarbon*, 35(1), 215–230, 1993.

812 Stuiver, M., Grootes, P. M. and Braziunas, T. F.: The GISP2  $\delta^{18}\text{O}$  Climate Record of the Past  
813 16,500 Years and the Role of the Sun, Ocean, and Volcanoes, *Quat. Res.*, 44(3), 341–354,  
814 doi:10.1006/qres.1995.1079, 1995.

815 Sun, Y., Clemens, S. C., Morrill, C., Lin, X., Wang, X. and An, Z.: Influence of Atlantic meridional  
816 overturning circulation on the East Asian winter monsoon, *Nat. Geosci.*, 5(1), 46–49,  
817 doi:10.1038/ngeo1326, 2012.

818 Sung, M.-K., Kwon, W.-T., Baek, H.-J., Boo, K.-O., Lim, G.-H. and Kug, J.-S.: A possible impact  
819 of the North Atlantic Oscillation on the east Asian summer monsoon precipitation, *Geophys. Res.*  
820 *Lett.*, 33(21), L21713, doi:10.1029/2006GL027253, 2006.

821 Tarasov, P. E., Bezrukova, E. V. and Krivonogov, S. K.: Late Glacial and Holocene changes in  
822 vegetation cover and climate in southern Siberia derived from a 15 kyr long pollen record from  
823 Lake Kotokel, *Clim. Past*, 5(3), 285–295, doi:10.5194/cp-5-285-2009, 2009.

824 Tauxe, L.: Sedimentary records of relative paleointensity of the geomagnetic field: theory and  
825 practice, *Rev. Geophys.*, 31(93), 319–354, 1993.

826 Timmermann, A., Lorenz, S. J., An, S.-I., Clement, A. and Xie, S.-P.: The Effect of Orbital Forcing  
827 on the Mean Climate and Variability of the Tropical Pacific, *J. Clim.*, 20(16), 4147–4159,  
828 doi:10.1175/JCLI4240.1, 2007.

829 Walker, M. J. C., Berkelhammer, M., Björck, S., Cwynar, L. C., Fisher, D. A., Long, A. J., Lowe, J.  
830 J., Newnham, R. M., Rasmussen, S. O. and Weiss, H.: Formal subdivision of the Holocene  
831 Series/Epoch: a Discussion Paper by a Working Group of INTIMATE (Integration of ice-core,  
832 marine and terrestrial records) and the Subcommittee on Quaternary Stratigraphy (International  
833 Commission on Stratigraphy), *J. Quat. Sci.*, 27(7), 649–659, doi:10.1002/jqs.2565, 2012.

834 Wang, Y., Cheng, H., Edwards, R. L., An, Z., Wu, J., Shen, C.-C. and Dorale, J. A.: A high-  
835 resolution absolute-dated late Pleistocene Monsoon record from Hulu Cave, China., *Science*,  
836 294(5550), 2345–8, doi:10.1126/science.1064618, 2001.

837 Wang, Y., Cheng, H., Edwards, R. L., He, Y., Kong, X., An, Z., Wu, J., Kelly, M. J., Dykoski, C.  
838 A. and Li, X.: The Holocene Asian monsoon: links to solar changes and North Atlantic climate.,  
839 *Science*, 308(5723), 854–857, doi:10.1126/science.1106296, 2005.

840 Wang, Y., Cheng, H., Edwards, R. L., Kong, X., Shao, X., Chen, S., Wu, J., Jiang, X., Wang, X.  
841 and An, Z.: Millennial- and orbital-scale changes in the East Asian monsoon over the past 224,000  
842 years., *Nature*, 451(7182), 1090–1093, doi:10.1038/nature06692, 2008.

843 Wu, B. and Wang, J.: Winter Arctic Oscillation, Siberian High and East Asian Winter Monsoon,  
844 *Geophys. Res. Lett.*, 29(19), 3-1-3–4, doi:10.1029/2002GL015373, 2002.

845 Xue, F., Wang, H. and He, J.: Interannual Variability of Mascarene High and Australian High and  
846 Their Influences on East Asian Summer Monsoon, *J. Meteorol. Soc. Japan*, 82(4), 1173–1186,  
847 doi:10.2151/jmsj.2004.1173, 2004.

848 Yu, J., Anderson, R. F., Jin, Z., Rae, J. W. B., Opdyke, B. N. and Eggins, S. M.: Responses of the

849 deep ocean carbonate system to carbon reorganization during the Last Glacial–interglacial cycle,  
850 *Quat. Sci. Rev.*, 76, 39–52, doi:10.1016/j.quascirev.2013.06.020, 2013.

851 Yu, Y., Yang, T., Li, J., Liu, J., An, C., Liu, X., Fan, Z., Lu, Z., Li, Y. and Su, X.: Millennial-scale  
852 Holocene climate variability in the NW China drylands and links to the tropical Pacific and the  
853 North Atlantic, *Palaeogeogr. Palaeoclimatol. Palaeoecol.*, 233(1–2), 149–162,  
854 doi:10.1016/j.palaeo.2005.09.008, 2006.

855 Yuan, D., Cheng, H., Edwards, R. L., Dykoski, C. A., Kelly, M. J., Zhang, M., Qing, J., Lin, Y.,  
856 Wang, Y., Wu, J., Dorale, J. A., An, Z. and Cai, Y.: Timing, duration, and transitions of the last  
857 interglacial Asian monsoon., *Science*, 304(5670), 575–578, doi:10.1126/science.1091220, 2004.

858 Zijderveld, J. D. A.: A. C. demagnetization of rocks : analysis of results, in *Methods in*  
859 *Palaeomagnetism*, edited by D. W. Collinson, K. M. Creer, and S. K. Runcorn, pp. 254–286,  
860 Elsevier., 1964.

861

862

863

864 **Captions**

865 Table 1. AMS <sup>14</sup>C data in monospecies planktic foraminifera *N. pachyderma* sin. and benthic  
866 foraminifera *Epistominella pacifica* and *Uvigerina parvocostata* of core 41-2. All measured AMS  
867 <sup>14</sup>C data were calibrated by Calib 6.0 (Stuiver and Reimer, 1993) with Marine13 calibration curve  
868 (Reimer et al., 2013) with a surface water reservoir ages of 900 years (Max et al., 2014). In the case  
869 of using benthic foraminifera for dating, we accept that the difference in paired benthic-planktic  
870 foraminifera ages equals 1,400 years, based on unpublished data and total regional results of Max et  
871 al. (2014). All radiocarbon ages were converted into calibrated 1-sigma calendar age.

#	Lab. code	core depth cm	foraminifera species	<sup>14</sup> C- age year	Err.1 sigma year	calendar age, ka
1	YAUT-021713	120	<i>E. pacifica</i>	10078	47	9.121
2	YAUT-021714	127.5	<i>E. pacifica</i>	10340	42	9.445
3	UCIAMS- 148095	298	<i>N. pachyd.</i>	13160	50	14.393
4	UCIAMS- 148096	156	<i>Uv. parvoc.</i>	11135	45	10.60
5	UCIAMS- 148098	306	<i>Uv. parvoc.</i>	14185	35	14.616

872

873

874 Table 2. Centennial events with increased / decreased productivity during 25-8 ka in core 41-2 and  
875 the average ages according to the correlations between productivity events and the EASM sub-  
876 interstadials and sub-stadials (CsI/CsS).

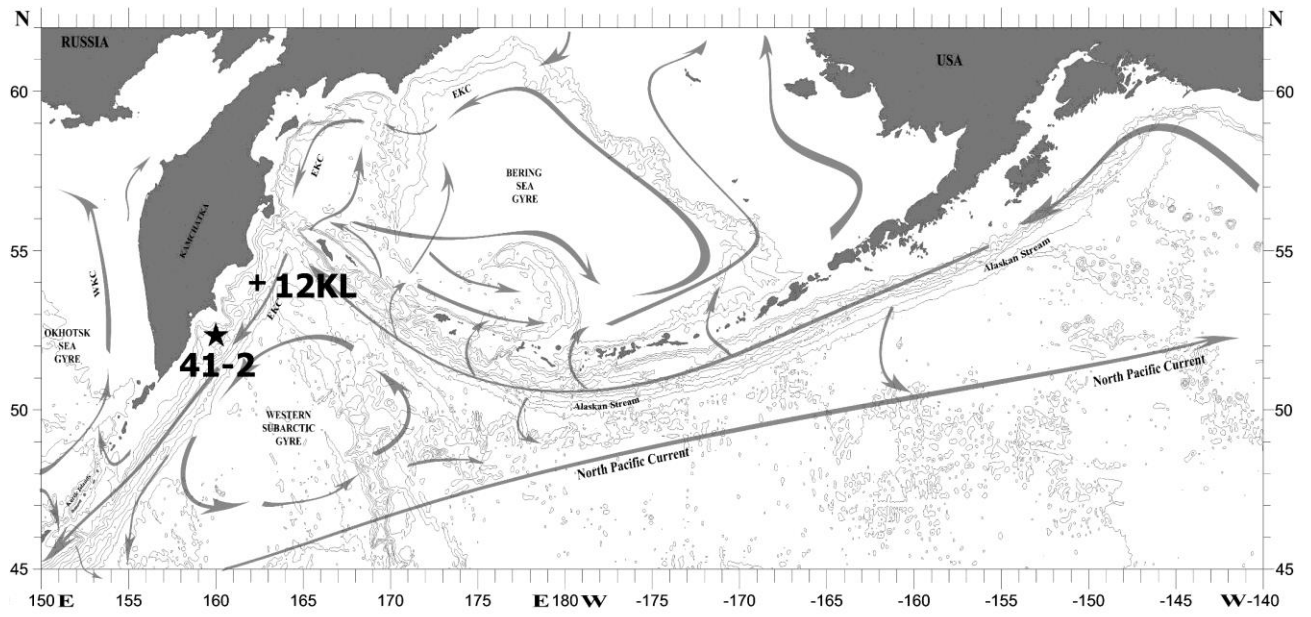
Events	Core interval, cm	Averaged cal. age, ka
CsS-EH-1	105-110	8.2
CsI-EH-1	111-116	8.6
CsS-EH-2	117-123	9.1
CsI-EH-2	124-129	9.5
CsS-EH-3	131-140	9.9
CsI-EH-3	141-153	10.5
CsS-EH-4	155-167	11.1
CsI-EH-4	168-181	11.5
CsI-GI1-a	231-238	13.1
CsI-GI1-c1	248-262	13.5
CsI-GI1-c3	269-279	13.8
CsI-GI1-e	285-306	14.3
CsI-GS2.1-1	317-322	14.9
CsI-GS2.1-2	335-339	15.5
CsI-GS2.1-3	353-360	16.5
CsI-GS2.1-4	373-381	17.5
CsI-GS2.1-5	388-395	18.1
CsI-GS2.1-6	399-407	18.6
CsI-GS2.1-7	420-425	19.2
CsI-GS2.1-8	432-437	19.5

877

878

880 Table 3. The age controlling points of core 41-2 derived from available AMS <sup>14</sup>C data of core 41-2,  
 881 projection of AMS <sup>14</sup>C ages of core 12KL, and tie points through correlation between increased  
 882 productivity events and EASM CsIs (Wang et al., 2008). One AMS <sup>14</sup>C datum of core 12KL at depth  
 883 of 706 cm was accepted according to the Tiedemann/Max age model 2 (Max et al., 2012, 2014).

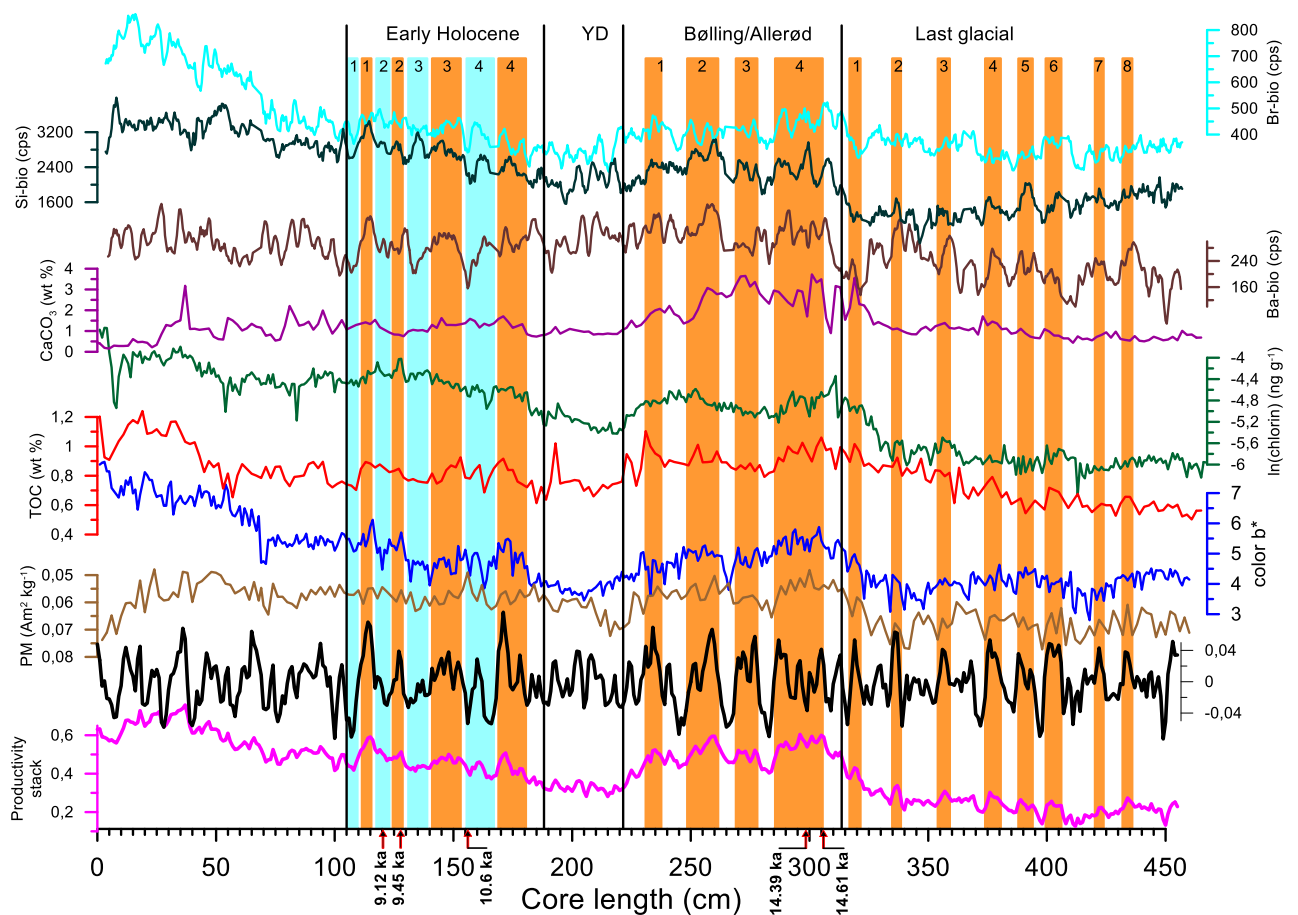
Depth	AMS <sup>14</sup> C core 41-2	Key time points of core 12KL	correlation with ages of China subInterstadial	Accepted key time points
cm	Cal. age, ka	ka/ depth (cm)		Cal. age, ka
120	9.12			9.12
127.5	9.45			
126		9.51/210		9.51
156	10.6			
159		11.08/295		11.08
167		11.31/340		11.31
234			13.08/GsI-GI1-a	13.08
251		13.42/508		13.42
273		13.79/550		13.79
298	14.39			
303		14.42/611		14.42
306	14.61			
337			15.42/CsI-GS2.1-2	15.42
348		16.16/706		16.16
357			16.51/ CsI-GS2.1-3	16.51
379			17.56/ CsI-GS2.1-4	17.56
393			18.12/ CsI-GS2.1-5	18.12
402		18.6/821		18.6
405			18.78/ CsI-GS2.1-6	18.78
423			19.25/ CsI-GS2.1-7	19.25
434		19.54/876		19.54



886

887 Fig. 1. Bathymetry, surface water currents and location of the cores 41-2 (star) and 12KL (cross)  
 888 (Max et al., 2012) in the N Pacific. Surface currents as in (Favorite et al., 1976) with modifications.  
 889 EKC – East Kamchatka Current, WKC – West Kamchatka Current.

890

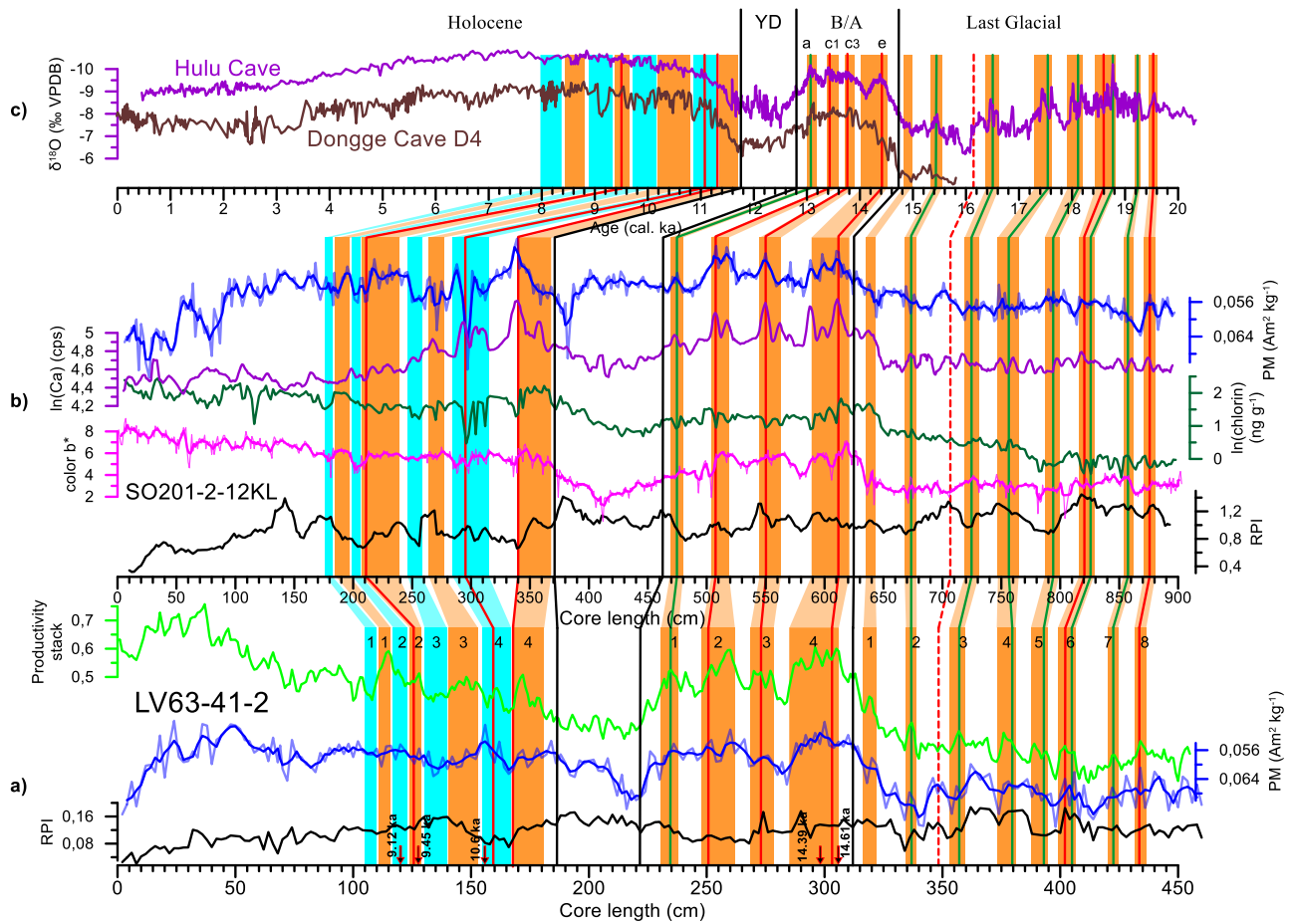


891

892 Fig. 2. Records (from bottom to top) of the original and detrended productivity stacks, PM, color b\*,  
 893 TOC, chlorin, CaCO<sub>3</sub>, Ba-bio, Si-bio, and Br-bio versus depth. Preliminary boundaries of the B/A  
 894 warming, YD cooling, and Holocene are shown according to general variability of productivity in the  
 895 NW Pacific, Sea of Okhotsk, and Bering Sea (Galbraith et al., 2007; Gorbarenko, 1996; Gorbarenko  
 896 and Goldberg, 2005; Keigwin, 1998; Seki et al., 2004). AMS <sup>14</sup>C data (calendar ka) are shown at the  
 897 base. Blue bars indicate cold periods / lower productivity events. Orange bars indicate warm periods  
 898 / high productivity events.

899

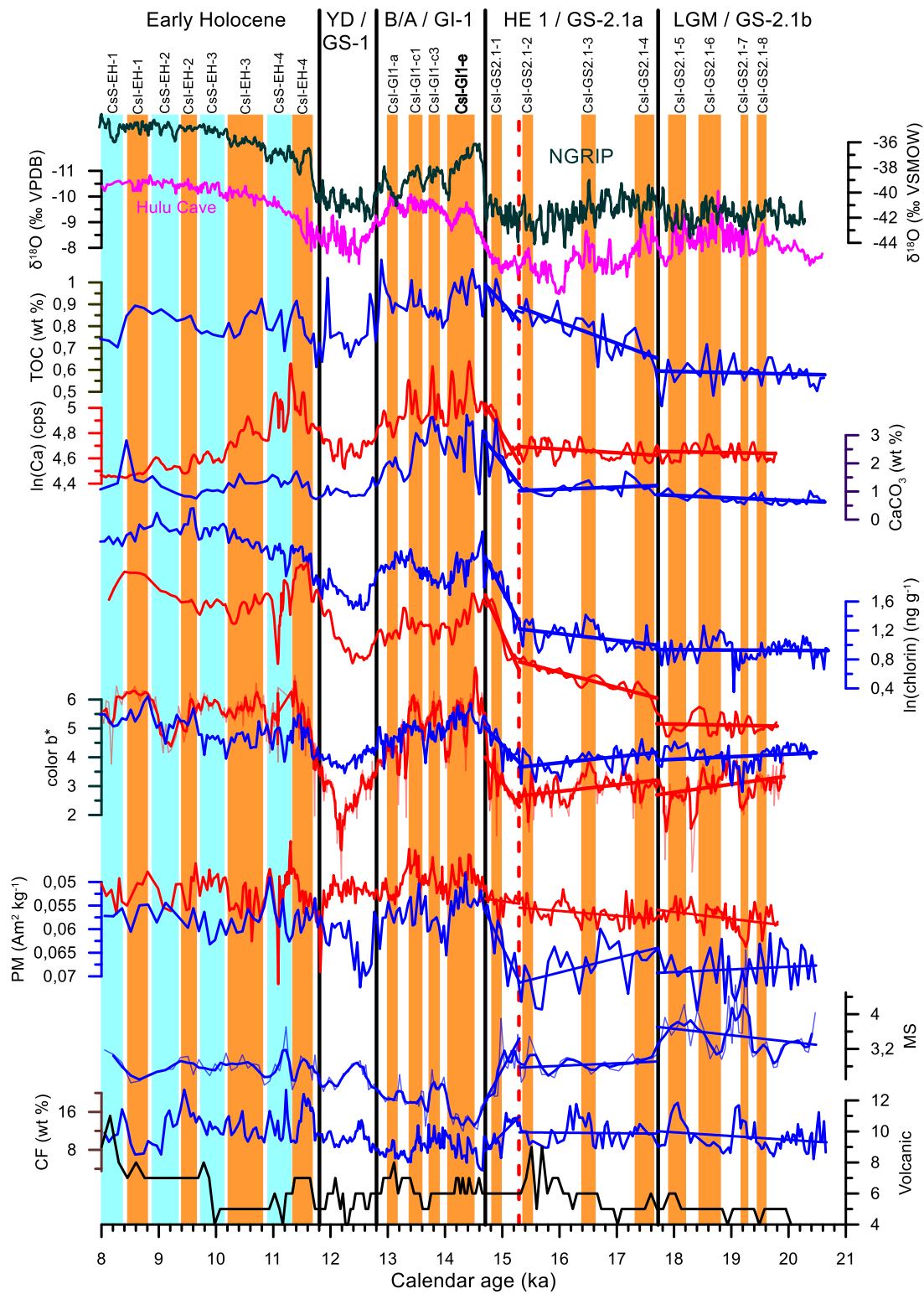




900

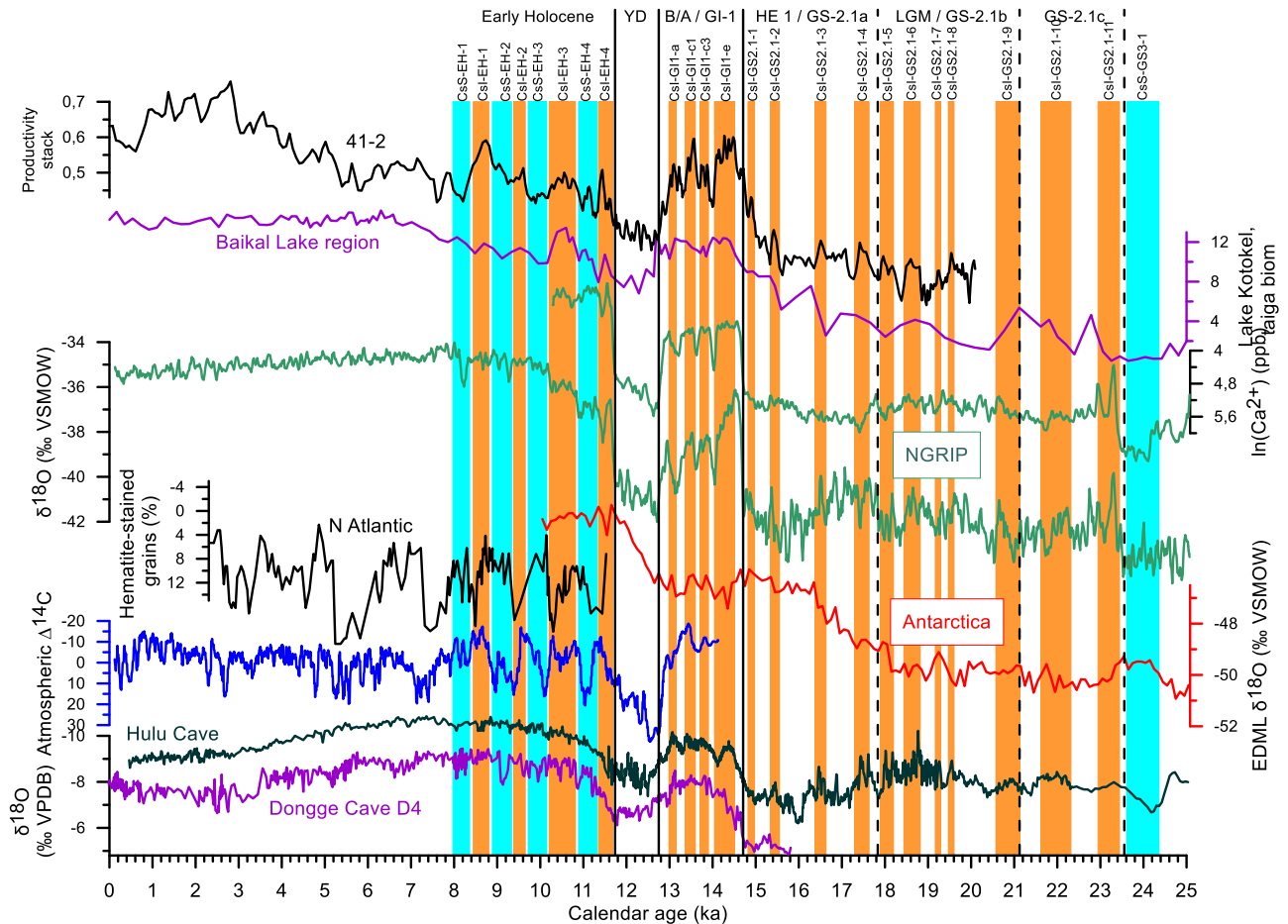
901 Fig. 3. Age model of core 41-2. Low panel: (a) RPI, PM and productivity stack of core 41-2 versus  
 902 depth. (b) Middle panel: RPI, color b\*, chlorin, Ca and PM of core 12KL versus depth. (c) Upper  
 903 panel:  $\delta^{18}\text{O}$  calcite of Chinese cave stalagmites (Dykoski et al., 2005; Wang et al., 2008) over the last  
 904 20 ka. The correlation of productivity events between core 41-2 and 12KL was established according  
 905 to correlation of productivity stack of core 41-2 with productivity proxies of core 12KL and the RPI  
 906 records of both cores. AMS  $^{14}\text{C}$  data of core 12KL (red lines) were projected to the core 41-2  
 907 according to correlated productivity events. A close correlation of the productivity events with sub-  
 908 interstadials in the EASM becomes apparent after projection of the radiocarbon data on the age scale  
 909 of EASM. Green lines correlate EASM sub-interstadials with productivity events. Orange and blue  
 910 bars are as in Fig. 2.

911



912

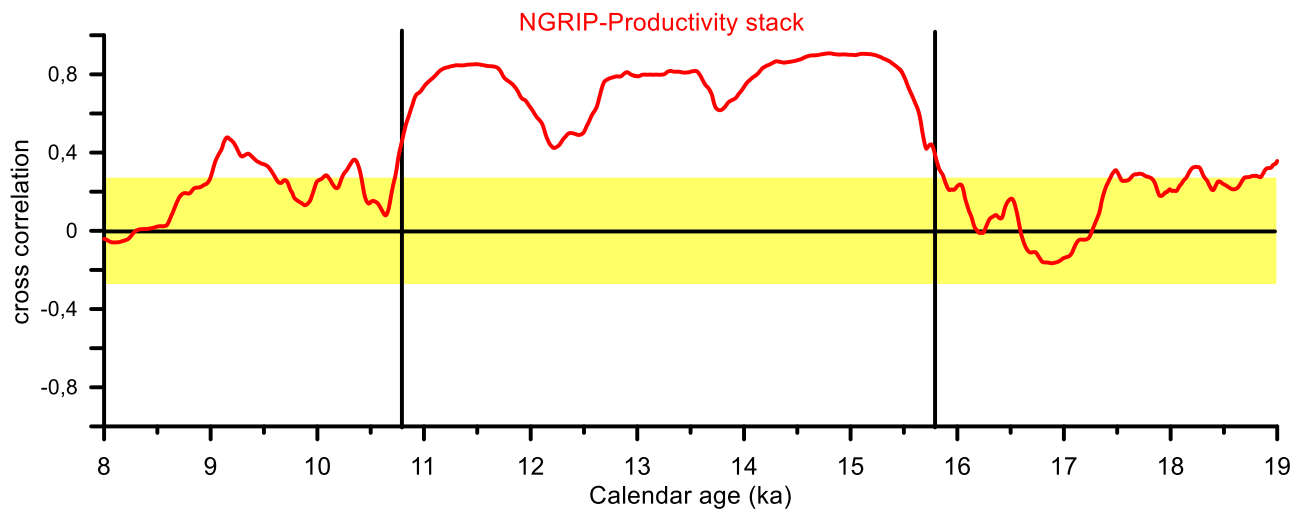
913 Fig. 4. High resolution variability of the productivity and lithologic proxies in the NW Pacific during  
 914 21–8 ka. Volcanic particles, CF, MS, PM, color b\*, chlorin, CaCO<sub>3</sub>/Ca, and TOC determined in cores  
 915 41-2 (blue lines) and 12KL (red lines) are shown from bottom to top. Δ18O records of EASM (Wang  
 916 et al., 2008) and NGRIP (North Greenland Ice Core Project members, 2004) are shown at the top of  
 917 the figure. Linear trends are shown for productivity and lithologic proxies during 20-17.8, 17.8-15.3,  
 918 and 15.3-14.7 ka periods. Red dashed line marks the boundary in productivity and lithologic trends  
 919 during HE1 at 15.3 kyr. Orange and blue bars are as in Fig. 2.



921

922 Fig. 5. Compilations of Northern and Southern Hemisphere climate records, solar activity, NW  
 923 Pacific productivity events, and vegetation records from the southern Siberia during the last 25 ka.  
 924 From bottom to top: absolutely dated  $\delta^{18}\text{O}$  calcite of Chinese cave stalagmites (Dykoski et al., 2005;  
 925 Wang et al., 2008); the residual atmospheric  $\Delta^{14}\text{C}$  record of around 2000-year moving average  
 926 (Reimer et al., 2004);  $\delta^{18}\text{O}$  EDML records after methane synchronization with the N Greenland ice  
 927 core (EPICA Community Members, 2006); the petrologic tracer of drift ice in the N Atlantic (Bond  
 928 et al., 2001); the  $\delta^{18}\text{O}$  and  $\text{Ca}^{2+}$  records in the Greenland NGRIP ice core indicated air temperature  
 929 and dust variability on GICC05 age scale (Rasmussen et al., 2014), pollen reconstructed Southern  
 930 Siberia environment changes (Lake Baikal region) (Bezrukova et al., 2010) and productivity stack  
 931 for core 41-2. Orange and blue bars are as in Fig. 2. Centennial events with increased productivity  
 932 are associated with sub-interstadial of the EASM and with increasing input of solar irradiance during  
 933 the LGM-B/A and EH short-term warmings, respectively. The correlation between short-term  
 934 increased Greenland temperature (NGRIP ice core) and a decreased Antarctic temperature is less  
 935 pronounced but seems to be marked as well.

936



937

938 Fig. 6. Cross correlation (CC) of the NW Pacific productivity stack and  $\delta^{18}\text{O}$  records of the NGRIP  
 939 (Rasmussen et al., 2014), using moving windows at 2000 years. Yellow bars depict the CC within  
 940 range  $\pm 0.25$ . Vertical black lines distinguish an interval from 10.8 to 15.8 ka with significant CC  
 941 (from -0.6 to -0.9) from less significant CC during earlier and later intervals indicating the  
 942 synchronicity climate changes between the N Atlantic and NW Pacific.